A MODEL TO PREDICT OIL/WATER EMULSION PHASE INVERSION IN THE DOWNHOLE ENVIRONMENT

By

SIVAKUMAR SAMBASIVAM

Bachelor of Technology

Bharathiar University

Coimbatore, India

1990

Submitted to the Faculty of the
Graduate College of the
Oklahoma State University
in partial fulfillment of
the requirements for
the Degree of
MASTER OF SCIENCE
May, 1994

OKLAHOMA STATE UNIVERSITY

A MODEL TO PREDICT OIL/WATER
EMULSION PHASE INVERSION
IN THE DOWNHOLE
ENVIRONMENT

Thesis Approved:

Alan Sill
Thesis Adviser

Martin S. High

Arland H. Johannes

Thomas C. Collins
Dean of the Graduate College

ACKNOWLEDGMENTS

Quite a few people deserve my thanks for their support, encouragement and advice. I wish to express sincere gratitude to my adviser, Dr. Alan D. Tree, for his inspiration, motivation, and guidance. I also appreciate his patience in going through the thesis corrections meticulously to offer suggestions. I am also thankful to my committee members, Dr. A. H. Johannes and Martin S. High for their suggestions and support.

I am greatly indebted to Dr. Lionel Raff and Dr. Guohai Liu for their invaluable help and technical assistance rendered towards this thesis work. My acknowledgments is due to all the industrial sponsor's for their financial support through the School of Chemical Engineering.

I am deeply grateful to my dearest parents, Sambasivam, V. and Jayalakshmi, S., brother Jayaprakash, and sister Sripriya, for their encouragement, support, understanding and confidence through thick and thin. Special thanks to Chitra for her affectionate and understanding nature making me feel at home.

I thank in no less terms my friends Ramasubbu, John, Thumbs, Nat, Suchu, JD and Sai without whom this endeavor would not have been as educational and stimulating.

TABLE OF CONTENTS

Chapter		Page
I.	INTRODUCTION	1
	Thesis Organization	4
II.	LITERATURE REVIEW	5
	Background	5
	Formation of Emulsions	9
	Stability of Emulsions	11
	Droplet Breakage and Size Determination	14
	Distribution of Drop Size	21
	Phase Inversion	27
III.	MODEL DEVELOPMENT	31
	Physical Model	32
	Determination of Drop Size	34
	Distribution of Drop Size	40
	Prediction of the Location	47
	Numerical Aspects of the Model	47
	Summary	48
IV.	RESULTS AND DISCUSSION	53
V.	CONCLUSIONS AND RECOMMENDATIONS	74
REFERENCES		77
APPENDIXES		83
APPENDIX A:	NOMENCLATURE	84
APPENDIX B:	OPERATING INSTRUCTIONS OF THE CODE	88
APPENDIX C:	COMPUTER CODE LISTING TO PREDICT THE POINT OF EMULSION PHASE INVERSION	90

LIST OF TABLES

Table Page

1. Input Data for Two Extreme and a Normal Case with respect to the strength of the Flow field 53

LIST OF FIGURES

Figure		Page
1.	Size Frequency Curves of Droplets of some Emulsions (1-4) made in the Model.....	23
2.	Drop Size Distribution Curve for a 10% Dispersion Flowing at 6 gal/min through Orifice Diameter of 0.375 inch	23
3.	Temperature and Oil Phase Volume Fraction, and Experimental Paths, for which the Emulsion Morphology remained Unchanged: Circles, O/W Morphology; Squares, W/O Emulsions	29
4.	Schematic Diagram of Downhole Annular Two-Phase Gas/Liquid Flow	33
5.	General Algorithm Flowsheet to Predict the Inversion Point	51
6.	Monte Carlo Method Flowsheet to Determine the Drop Size Distribution of the Emulsion	52
7.	Histogram of Drop Size Distribution of Water Droplets (Case 1).	56
8.	Histogram of Drop Size Distribution of Water Droplets (Case 2).	58
9.	Histogram of Drop Size Distribution of Water Droplets (Case 3)	59
10.	Histogram of Drop Size Distribution of Oil Droplets (Case 3)	60
11.	Drop Size Distributions as a Function of the Second Invariant of Water-in-Oil Emulsion.	62

Figure Page

12. Surface Energy as a Function of Number of Monte Carlo Moves for $f(\dot{\gamma}_{w/o}) = 0$ and Water Dispersed in Oil. 64

13. Surface Energy as a Function of Number of Monte Carlo Moves for $f(\dot{\gamma}_{w/o}) = 1$ and Water Dispersed in Oil. 65

14. Surface Energy as a Function of Number of Monte Carlo Moves for $f(\dot{\gamma}_{w/o}) = 1x10^{-14}$ and Water Dispersed in Oil 66

15. Surface Energy as a Function of Number of Monte Carlo Moves for $f(\dot{\gamma}_{o/w}) = 1x10^{-15}$ and Oil Dispersed in Water 67

16. Phase Inversion Map (Equal Second Invariants of Water-in-Oil and Oil-in-Water Emulsion). 70

17. Phase Inversion Map (Different Second Invariants of Water-in-Oil and Oil-in-Water Emulsion). 71

CHAPTER I

INTRODUCTION

Corrosion is a serious and complex problem in oil and gas wells since the well tubing may fail unexpectedly due to corrosion, causing considerable expense in down time and replacement of the tubing. The complexities of corrosion behavior are so great that it is difficult, if not impossible, to outline a simple method for evaluating and predicting corrosion in all wells. Rowe and Waldrip (1958) on their study in the corrosivity of oil and gas wells said that corrosion in oil wells, especially in condensate producers, is often very erratic and may be concentrated at the bottom, center, or at the top of the tubing or even throughout the string in some cases.

The corrosion engineer needs to understand the corrosion mechanics in order to choose the control method that gives adequate protection at an acceptable cost. The goal of this work is to provide a better understanding of the complex nature of oil and gas well corrosion in order to prevent unnecessary production expenses.

Among the different types of corrosion, the two most commonly encountered in oil and gas wells are uniform corrosion and localized corrosion. Uniform corrosion is

the general thinning of the metal or overall loss due to chemical or abrasive action and localized corrosion is the formation of pits or grooves in the pipe wall. Other types of corrosion such as erosion-corrosion, hydrogen embrittlement and stress corrosion cracking are seen less frequently. Both uniform and localized corrosion are very common in oil and gas wells.

Uniform or localized corrosion in gas wells is predominantly due to liquid water contacting the metal surface. Other factors influencing the location and rate of corrosion in an oil or gas well are the presence of acid gases CO_2 or H_2S; the presence of solid contaminants; pressure; temperature; pH and the presence of oxygen. Corrosion rates are particularly aggravated by high concentrations of the acid gases in solution with the liquid water phase. If the corrosion engineer can predict the length along the well bore at which the tubing will become waterwet the appropriate action can be taken to prevent the corrosion.

In a previous corrosion study, a model for uniform corrosion in gas wells with and without a carbonate film was formulated by Liu (1991). The Liu model assumes that corrosion begins wherever liquid water is present in the gas well. However, corrosion actually begins only when the water phase is in contact with the metal surface. Hence, the presence of an oil phase on the well wall may protect the metal surface. Since the gas flows at a very

high rate, the water and oil on the tubewall can be expected to be in highly turbulent flow which would form an emulsion. The possibility of corrosion protection due to the presence of an emulsion was not considered in the Liu model.

Emulsions considered in this work may be of two types, water-in-oil emulsions or oil-in-water emulsions. Water-in-oil emulsions consist of water droplets encapsulated in a continuous oil phase, whereas, oil-in-water emulsions consist of oil as the dispersed phase in a continuous water phase. The type of emulsion present depends on local conditions such as relative amounts of water and oil; temperature and gas velocity. Since the conditions in the well vary with depth, inversion points may be expected at which the emulsion type changes.

The purpose of this thesis is to develop a model that will more precisely predict the location where corrosion begins in a gas well by determining under what condition a water-in-oil emulsion will convert to a potentially corrosive oil-in-water emulsion. The system considered was a three-phase annular flow with a gas phase flowing in the core and a two-phase liquid film along the walls of the tubular. This liquid film may be in the form of either a water-in-oil or an oil-in-water emulsion. Corrosion is assumed to occur only when the water displaces the oil phase and wets the tubing. A Monte Carlo simulation was used to model the emulsions.

Thesis Organization

Chapter II is a literature review which surveys the behavior of emulsions, the Monte Carlo technique, and derivations of drop diameters of emulsions needed for the Monte Carlo simulation. Chapter III presents the development of the Monte Carlo simulation in detail. Chapter IV gives the simulation results and discusses the phase inversion predictions. Chapter V summarizes the major results and gives guidelines for continuation of this work.

CHAPTER II

LITERATURE SURVEY

This chapter gives an overview of the literature on the topics relevant to this work. In particular, the background of downhole corrosion rate calculations; formation, stability of emulsions; minimum and maximum drop size of emulsions; the Monte Carlo method to determine the drop size distribution; and the phase inversion of emulsions are reviewed.

Background

A survey of the literature shows that several parameters affect the downhole corrosion rate in gas wells including the amount of CO_2 and H_2S present in the gas phase; temperature and pressure; the presence of solid contaminants; the properties of corrosion product film; the fluid velocity; the type of flow regime (e.g., bubble, slug, annular, etc.); the concentration of various inorganic ions in the formation water; and the gas and water production rates.

Some authors (Shock & Sudbury 1951, Zitter 1973, Smith 1982, Tuttle 1988, 1990) believe that the partial

pressure of CO_2 and H_2S are the most important factors in predicting the corrosion rate of a well. According to these authors' wells can be classified as corrosive if the partial pressure of the corrosive gases is above 15 psi, probably corrosive if the partial pressures are between 7 psi and 15 psi, and non corrosive for partial pressures less than 7 psi.

Bradburn (1977) found that water production was a better indicator of corrosion rates than the partial pressure of corrosive gases. Later authors (Gatze & Hausler 1984, Hausler & Burke 1985) included the gas production rate as another factor in addition to the water production rate. The later authors also concluded that the partial pressures of the acid gases and total solids in the brine are only minor factors compared to the gas production rate.

Crolet (1983) and Crolet & Bonis (1984) proposed that the physical chemistry of water and the two-phase flow pattern (e.g., slug flow, mist flow, annular flow, etc.) are other factors that, in addition to fluid velocity, affect the corrosion rate. The experiments done by the above authors showed that production water containing a minimum amount of bicarbonate had a determining influence on water aggressivity. Johnson (1991) observed the severity of corrosion rates during slug flow. He found that the corrosion rate in wells experiencing slug flow was enhanced by a factor of 7 compared to annular flow.

Ideha et al. (1984) reported corrosion rates as a function of three distinct temperature regions: below 60°C (homogeneous corrosion attack), 100°C (maximum corrosion rate) and above 150°C (lower corrosion rate). Hausler (1984) however showed the corrosion rate is higher at 60°C than at either 90°C or 120°C. Valand & Sjowall (1989) and Choi, Chepulis & Lee (1989) also had different regions of temperature for maximum and minimum corrosion. The different experimental conditions (flow rates and mass transfer rates) of the above researchers could be a reason for the contradiction in the relation between the corrosion rate and temperature.

Electrochemical reaction mechanisms for the corrosion of steel by CO_2 solutions were proposed by Dewaard & Milliams (1975), Schmitt & Rothman (1977) and Wieckowski, Ghali & Szklarczyk (1983a, 1983b) based on experimentation. Kawashima, Hashimoto & Shimodaira (1976), Morris, Sampaleann & Veysey (1980) and Iyer, Takenchi & Zamanzadeh (1991) proposed mechanisms for corrosion of steel by H_2S in aqueous solutions that are similar to the surface mechanism of CO_2. Mass transfer also influences the corrosion rate and Ross & Badhwar, (1965) and Mahato & Shemilt, (1980) give correlation's between the wall roughness to the corrosion rate.

An apriori model considering all the above factors would be a boon to corrosion engineers. Robertson and Erbar (1988) made a first attempt to simulate downhole

corrosion; predict downhole pressure and temperature profiles; and phase behavior. The model determined the water condensation zone and the prevailing flow regime in the well. Similar work has been presented by Reinhardt and Powell (1988). However, Reinhardt and Powell assumed both the temperature and pressure profiles to be linear and did not account for two-phase flow regimes. The calculation of downhole corrosion rate was not considered by either of the models. However, these models were the foundation on which further models pertaining to corrosion rate calculations were developed.

Fang, Garbar, Perkins & Reinhardt (1989) from the University of Southwestern Louisiana have been developing a model for downhole corrosion which provides the temperature and pressure profiles of gas wells; condensed water and formation water calculations; phase equilibrium calculations; corrosion rates; and film thickness for annular two-phase flow. The Southwestern Louisiana State (SLS) model is oversimplified because only Fe^{++} ion transfer from pit to bulk liquid was considered. The model also assumes a linear temperature and pressure profile and the corrosion rate calculations do not involve the effect of the surface mechanisms and mass transfer rate. The SLS model uses an empirical correlation for the calculation of corrosion rate.

Liu and Erbar (1990) proposed a model where Hydrogen ion was assumed to be the key corrosive species when acid

gases are present. The concentration of Hydrogen ions was calculated through the dissociation equilibrium at the downhole temperature and pressure. This model predicted uniform corrosion without a protective film and made the first attempt to include the fluid dynamics, mass transfer and surface reaction mechanisms in a single model. Liu (1992) made further modifications with the inclusion of consideration of a protective film. Liu's model (1992) also increased the accuracy of pressure drop predictions. However, Liu's model assumes that corrosion begins where water first starts to condense in the gas well. However, one of the basic conditions for corrosion to occur is, that the water phase must be in contact with the metal surface (Crolet & Bonis, 1989). Hence the presence of the an oil phase on the pipe wall may prevent wetting and protect against corrosion since corrosion occurs only when the hydrocarbons are displaced by the water phase.

Formation of Emulsions

Emulsions can be found in almost every part of the petroleum production and recovery process: in reservoirs, at well heads, in many parts of the refining process, and in transportation pipelines. Most petroleum emulsions that are encountered in practice contain oil, water, and an emulsifying agent.

In the formation of petroleum emulsions, the two immiscible liquids in gas wells are oil and water and the emulsifying agents are the asphaltenes present in the oil. The turbulent flow of the gas in the pipelines provides the energy required for emulsification. In theory, the amount of energy required to increase the surface area by droplet breakup can be calculated if the interfacial tension between the two liquids is known (Becher, 1966).

Many methods for the measurement of interface tension, including the details of the experimental techniques and their limitations, are found in the literature. The spinning drop technique is applicable to the low interfacial tensions encountered in oil recovery and micro emulsion fields (Cayias et al, 1975). The interfacial tension used in the present work for oil and water emulsion was that of Benzene and water which is 30 dynes/cm (N.K. Adam, "Physics and Chemistry of Surfaces").

Emulsifying agents form a thin interfacial film which maintains the stability of the emulsion by minimizing the contact and aggregation of the internal phase. Bancroft's rule says that the emulsifying agent should be more soluble in the external phase such that the molecules are readily available for adsorption around the internal phase (Schramm, 1992). The emulsifying agent must have a molecular structure in which the polar end is attracted to the water and the non-polar end to the oil.

Most substances acquire a surface electric charge when brought into contact with a polar medium such as water. In a practical petroleum emulsion situation, the degree of surface charging is complicated. An example is the bitumen-water interface, which becomes negatively charged in alkaline aqueous solutions as a result of the ionization of surface carboxylic acid groups belonging to natural surfactants present in the bitumen. The degree of negative charging depends on the pH and ionic strength of the solution (Takamura et al., 1983) and also on the concentration of natural surfactant monomers present in the aqueous phase.

Stability of Emulsions

The stability of an emulsion can be defined as the resistance of the emulsion droplets to being broken or coalescing. Stability depends on factors like the overall water content, emulsifying agent and viscosity. An increase in the water content leads to a larger number of water droplets per unit volume and a higher rate of droplet collision; ultimately forming large droplets and leading to the breakdown of the emulsion.

The function of the surfactant is to avoid rupture or coalescence of the droplet. Depending on the chemical composition of the surfactant, emulsion stability can either increase or decrease. Materials containing mono-

valent ions have been shown to stabilize the oil-in-water emulsions and materials with poly-valent ions stabilize water-in-oil emulsions.

An important property of an emulsion is the shear viscosity. Factors like the temperature, volume, viscosity of dispersed phase and the emulsifying agent affect the viscosity of the emulsion. A continuous oil phase with a high viscosity will yield a more stable emulsion because the movement of the droplets is much slower. However, if the temperature increases the viscosity will decrease (Pal & Rhodes, 1985) and the probability of collision will increase leading to de-stabilization of the emulsion.

The volume fraction of the dispersed phase is the most important factor that affects the viscosity of emulsions. When particles are introduced into a given flow field, the flow field becomes distorted, and consequently the rate of energy dissipation increases, leading to an increase in the viscosity of the system. Einstein (1911) showed the increase in the viscosity of the system due to the addition of particles as a function of the volume fraction of the dispersed particles.

Pal and Rhodes (1989) developed a viscosity-concentration relationship for emulsions as a function of the dispersed phase concentration and shear rate:

$$\eta_r = 1 + \left[\frac{\phi / \phi_{\eta_r=100}}{1.187 - \phi / \phi_{\eta_r=100}} \right]^{2.492} \qquad \text{(II-1)}$$

where η_r is the relative viscosity of the emulsion (ratio of the viscosity of the emulsion to that of the continuous phase); ϕ is the dispersed phase volume fraction; and $\phi_{\eta_r=100}$ is the dispersed phase concentration at which the relative viscosity becomes 100. The term $\phi_{\eta_r=100}$ takes into account the system to system variations such as the type of emulsion system, temperature, shear rate, etc., and is calculated from experimental shear stress versus shear rate data. Equation (II-1) can be applied only for dispersed phase concentrations less than 74% by volume.

The viscosity of an emulsion also depends upon the viscosity of the dispersed phase; particularly when internal circulation occurs within the dispersed droplets. The presence of internal circulation reduces the distortion of the flow field around the droplets (Sherman, 1968), and consequently the overall viscosity of an emulsion is lower than that of a suspension at the same volume fraction. With the increase in dispersed-phase viscosity, the internal circulation is reduced, and consequently the viscosity of the emulsion increases.

The presence of an emulsifier greatly inhibits internal circulation (Sherman, 1970), and the emulsion

droplets behave more like rigid particles. The chemical nature and the concentration of an emulsifying agent also play a role in determining the viscosity of emulsions (Sherman, 1968). The average particle size, particle size distribution, and the viscosity of the continuous phase all depend upon the properties and concentration of the emulsifying agent. Also, ionic emulsifiers introduce electroviscous effects, leading to an increase in the emulsion viscosity.

Droplet Breakage and Size Determination

This section deals with the droplet breakage mechanism and droplet diameter determination as presented in the literature. Taylor (1932) was the first to consider the deformation and breakup of liquid drops in a flow field. He derived the theoretical equation:

$$d_{max} = \frac{\sigma}{a\mu_c}\left[\frac{16\mu_d + 16\mu_c}{19\mu_d + 16\mu_c}\right] \qquad \text{(II-2)}$$

where d_{max} is the maximum liquid drop diameter; a is the maximum velocity gradient in the flow field; σ is the interfacial tension; μ_c and μ_d are the viscosities of the continuous and dispersed phase, respectively. The above equation predicts increasing maximum drop diameter with increasing dispersed phase viscosity, but the effect is small since the viscosity group in brackets only varies

from 1.0 to 0.84 as the dispersed phase viscosity goes from 0 to infinity.

Clay (1940) experimentally investigated the drop sizes and drops size distribution of liquid-liquid dispersions. He used a photographic method and determined the various drop sizes in turbulent flow in a pipe. Clay used his data to discuss the two elementary processes, drop coalescence and drop breakup. The two possibilities of coalescence are either the drops coalesce on collision or the drops cling to each other for sometime and then coalesce. For the drop breakup, Clay again proposed two possibilities. The first was the bursting of the drop due to a velocity gradient as investigated by Taylor. The second type of bursting process occurs when the pressure at the surface of a drop locally falls to a certain value below the mean pressure causing a local deformation of the droplet surface in the form of a tiny protuberance, which may lead to separation of a small droplet.

All theories of bubble and drop breakage in liquid turbulence are based on a balance of the forces that are breaking and resisting the breakage of the bubble and drop. As stated by Levich (1962) the breakage of a drop or a bubble is due to differences of velocity, u, within the turbulent field. The velocity differences in the vicinity of the drop create turbulent stresses, τ, on the bubble or drop surface which act against the force of interfacial tension of the bubble or drop. The turbulent

stresses will cause the drop to break if the drop exceeds the surface tension forces, of magnitude σ/d , resisting breakage. The ratio of these two forces is defined as the Weber number:

$$We = \frac{\tau}{\sigma / d}. \qquad \text{(II-3)}$$

where We is the Weber number; σ is the surface tension and d is the diameter of the drop. Since the magnitude of τ in a turbulent flow field is finite and the surface tension force of a bubble or drop increases with decreasing bubble size, Kolmogoroff (1949) and Hinze (1955) postulated that in any turbulent flow field there will be a stable bubble or drop size, d_s. The value of d_s can be characterized by a critical value of the Weber number, We_{crit} ,

$$We_{crit} = \frac{\tau}{\sigma / d_s}. \qquad \text{(II-4)}$$

Breakage will occur at values of Weber number greater than We_{crit} , and values less than We_{crit} will result in stable bubble or drops.

Hinze (1955) demonstrated that the We_{crit} is dependent on the type of deformation and on the flow pattern surrounding the bubble or drop. He postulated several types of drop deformation specific to a local fluid flow field and calculated values of the We_{crit} ranging from 0.5 to ∞. For dispersion in liquid turbulence, Hinze has

shown that the We_{crit} is approximately 1 using the data of Clay (1940).

Turbulent stresses are proportional to the differences in velocity across a distance equal to d and are characterized by Kolmogoroff and Hinze as

$$\tau = \rho_c \bar{u}^2 . \qquad \text{(II-5)}$$

where ρ_c is the continuous phase density and $\bar{u}^2$ is the average velocity. The relative velocity term, $\bar{u}^2$, describes the turbulent pressure forces of eddies of size $l \sim d$ and is defined as the average of the square of the differences in velocity over a distance equal to the bubble or drop diameter. At any position within a turbulent flow field, a spectrum of eddy sizes responsible for breakage are of the same order of magnitude as the drop size. Velocity differences characteristic of an eddy much greater than d result in translation of the drop, while differences in the velocity of eddies much less than d only causes a small deformation of the surface of the drop that does not lead to breakage.

To find the functional form of the velocity term, $\bar{u}^2$, within a spectrum of eddy sizes, Hinze applied the theory of isotropic turbulence. The relative velocity term is assumed to be dependent on only the local energy dissipation per unit mass, ε, and is given by Batchelor (1959) as,

$$\bar{u}^2 \sim 2(\varepsilon d_s)^{2/3} . \qquad \text{(II-6)}$$

Combining the above three equations result in the following equation for d_s:

$$d_s = \left\{\frac{We_{crit}}{2}\right\}^{0.6} \left\{\frac{\sigma}{\rho_c}\right\}^{0.6} (\varepsilon)^{-0.4}. \qquad \text{(II-7)}$$

Equation (II-7) describes the stable bubble or drop size as a function of the local energy dissipated by the turbulence and the physical properties of the fluids.

Levich (1962) uses a different approach to the breakage theory than that of Kolmogoroff and Hinze, and derives an equation for drop size. Levich considered the balance of the internal pressure of the drop with the capillary pressure of the deformed drop. The dispersed phase density is included through the internal pressure force term, and the capillary pressure is determined from the shape of the deformed drop rather than the spherical drop. Levich approximates the surface tension force of a deformed bubble or drop using the geometry of a cylinder with height h, surface area A, and volume V. The surface tension pressure, F_σ, can be approximated by

$$F_\sigma \sim \frac{\sigma}{d} \sim \left(\frac{\pi h^2}{V}\right)\sigma. \qquad \text{(II-8)}$$

The value of h is determined from a force balance about a deformed drop. The pressure difference across the drop is estimated by the Bernoulli equation from the local flow around the bubble or drop,

$$\Delta p = \frac{\rho_c u_c^2}{2}. \qquad \text{(II-9)}$$

where Δp is the pressure drop and u_C, the continuous phase velocity. At steady state, the deformation caused by the force Δp must be balanced by the surface tension force,

$$\Delta p A \partial h + \sigma \partial A = 0. \qquad \text{(II-10)}$$

Since the volume of the drop is constant with deformation in shape of drop, the change in the surface area with respect to the height is given by,

$$\frac{dA}{dh} = \frac{d}{dh}\left(\frac{V}{h}\right) = -\frac{V}{h^2} = -\frac{A}{h}. \qquad \text{(II-11)}$$

Combining the above four equations gives an expression for h,

$$h \sim \frac{2\sigma}{\rho_c u_c^2}. \qquad \text{(II-12)}$$

The surface tension force of the deformed drop, using an equivalent spherical diameter for the volume, can now be written as

$$F_\sigma \sim \frac{\sigma^3}{d^3\left(\rho_c u_c^2\right)^2}. \qquad \text{(II-13)}$$

The internal pressure within the drop arises from the surrounding turbulence. Levich postulates for a drop that the pressure forces within the drop, $\rho_d u_d^2$ can be described by a momentum balance resulting in:

$$\rho_d u_d^2 \sim \rho_c u_c^2. \qquad \text{(II-14)}$$

where ρ_d is the dispersed phase density and u_d is the dispersed phase velocity. The ratio of the forces described by the equations (II-13) and (II-14) gives the Weber number.

For a bubble, Levich assumes that the gas is completely entrained by the liquid, and the fluctuating velocities of both the surrounding liquid and within the bubble are equal,

$$u_d = u_c . \qquad \text{(II-15)}$$

The above equation can be used to approximate the breakage stress,

$$F_\sigma \sim \rho_d u_d^2 \sim \rho_c u_c^2 . \qquad \text{(II-16)}$$

From this concept, a critical Weber number is defined as

$$We_{crit} = \frac{\tau}{\sigma / d_s}\left(\frac{\rho_d}{\rho_c}\right)^{\frac{1}{3}} . \qquad \text{(II-17)}$$

The Levich theory can be further developed to predict the maximum stable drop size:

$$d_s = \left\{\frac{We_{crit}}{2}\right\}^{0.6}\left\{\frac{\sigma^{0.6}}{\left(\rho_c^2 \rho_d\right)^{0.2}}\right\}(\varepsilon)^{-0.4} . \qquad \text{(II-18)}$$

Levich also arrived at the maximum and the minimum diameters of the drops possible when the flow field is tubular, the derivation of which are given in the Chapter III. The equations for the drop diameters are given by,

$$d_{max} = \left[\frac{\sigma}{k_f \rho v^2}\right]^{0.6}(\lambda_0)^{1.6} . \qquad \text{(II-19)}$$

and

$$d_{min} = 2\sqrt{\frac{\sigma\nu}{25\rho\upsilon_0^3}}. \qquad \text{(II-20)}$$

where k_f is a numerical coefficient based on flow conditions; ν, the kinematic viscosity; λ_0, the scale of an eddy at which the Reynolds number is unity; ρ, the density of the eddy; and υ_0, the characteristic eddy velocity.

The maximum and minimum drop size diameters that were derived are used as input data to the Monte Carlo method to determine the drop size distribution. The diameters form the upper and lower limit for the log normal distribution of the emulsions.

Distribution of Drop Size

This section explains the method used to determine the drop size distribution and experimental evidence that log-normal distributions are common among emulsion systems. The Monte Carlo method to determine the drop size distribution is also developed.

The drop size distribution for a liquid-liquid dispersion flowing in a pipe has not been well defined in the literature. Clay (1940) experimentally investigated the drop size distribution of dilute liquid-liquid dispersions (water, kerosene, glycerol, liquid paraffine,

propanol, methanol, etc.). Clay's experimental arrangement consisted of flow in the annulus between two coaxial cylinders, the inner cylinder rotating. Clay made runs with concentration as low as 3.8 volume percentage and as high as 12 percent. Clay observed that the drop diameters ranged between 2 and 240 microns. Figure 1 presents the size frequency curves of the droplets of some emulsions used in the model by Clay. The x-axis is the diameter, a, of drops and the y-axis, the logarithm of the number of droplets, log n(a), of the emulsion. The legend 1-4 are the different emulsion systems for which the distributions were determined. The distributions were all similar having a single mode that was skewed towards the lower diameters.

Scott et al. (1958) studied the formation of interfacial area when a mixture of water and kerosene was pumped through orifice diameters (0.3125" to 0.75") a pipe. The authors presented a drop size distribution for a 10% volume dispersion flowing at six gallons per minute through an orifice diameter of 0.375". Figure 2 shows the drop diameters ranged from 20 to 250 microns with a sharp peak at 50 microns.

Several other authors (Epstein 1947, Kottler 1950, Mugele & Evans 1951, Schwarz & Bezemer 1956, Rajagopal 1959, Daling et al. 1990), examined other flow systems and developed models and reported distributions with a

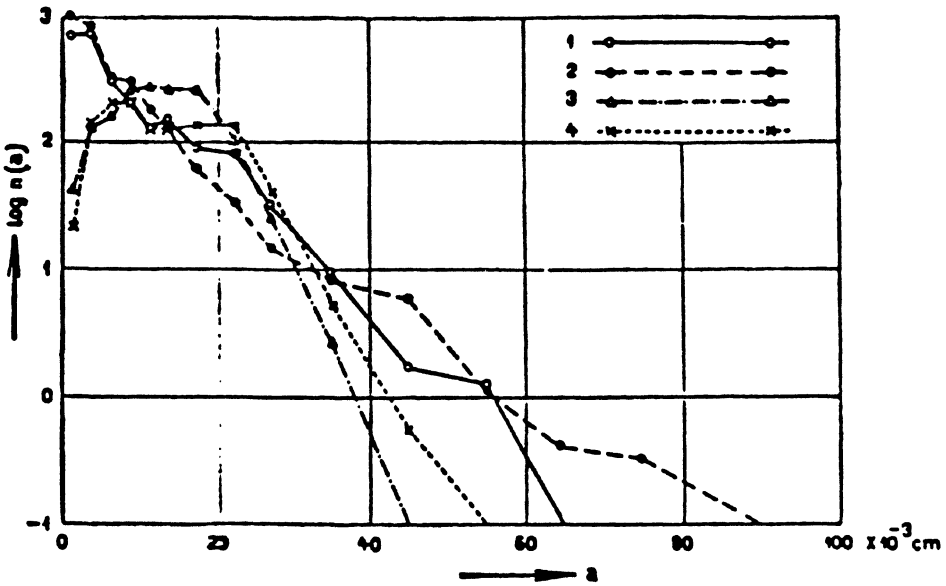

Figure 1. Size Frequency Curves of Droplets of some Emulsions (1-4) made in the Model (Clay, 1940)

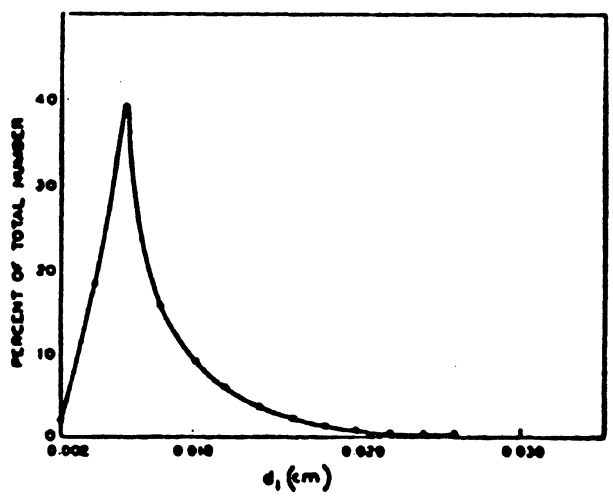

Figure 2. Drop Size Distribution Curve for a 10% Dispersion Flowing at 6 gal/min through Orifice Diameter of 0.375 inch. (Scott et al., 1958)

dividing the size range of the population into a number of increments and then counting the number of particles that fall into each interval. If the fraction of the total count that is found in an interval is plotted against the average size of the particles in the interval, a frequency diagram or histogram results. In the limit, as the number of particles becomes very large and the size of the increments very small, the histogram becomes a continuous curve, f(d), called the size-distribution of d.

One possible method to predict f(d) is the Monte Carlo technique which is a special numerical method involving random numbers. All Monte Carlo problems are solved by simulating the history of a large number of particles and by taking the average of the results thus estimating the solution to a specific problem.

Monte Carlo methods are mainly probabilistic or deterministic. A probabilistic Monte Carlo method is one which uses random numbers to simulate the actual situation and infer a solution from the behavior of the random processes. The deterministic Monte Carlo method is where the problem could be formulated theoretically but cannot be solved by theoretical means or is too cumbersome to solve mathematically.

Metropolis et al. (1953) developed the simplest method to calculate the equilibrium value of any system property of interest. N particles are placed in an arbitrary configuration, such as a regular lattice. Each

of the particles is allowed to move in succession according to the following equations:

$$X = X + \alpha\xi_1 . \qquad \text{(II-22)}$$

$$Y = Y + \alpha\xi_2 . \qquad \text{(II-23)}$$

$$Z = Z + \alpha\xi_3 . \qquad \text{(II-24)}$$

where α is the maximum allowed displacement and ξ_1, ξ_2, ξ_3 are randomly generated numbers between 0 and 1, exclusive. The change on energy of the system, ΔE, caused by the move is calculated. If $\Delta E < 0$, i.e. if the move would bring the system to a state of low energy, the move is allowed and the particle is put in its new position. If $\Delta E > 0$, the move is allowed with the probability $\exp(-\Delta E/RT)$. A random number between 0 and 1 is generated and if this random number, ξ is such that $\xi < \exp(-\Delta E/RT)$, the particle is moved to its new position. If $\xi > \exp(-\Delta E/RT)$, the move is rejected and the particle returns to its old position. Whether the move has been allowed or not, i.e., whether the configuration is new or old, it is considered to be a new configuration for the purpose of taking the averages. The average of any property, F_j is given by,

$$\bar{F} = \frac{1}{M} \sum_{j=1}^{M} F_j \qquad \text{(II-25)}$$

where M is the number of moves and F_j is the value of the property at the j^{th} move. The greater the number of

moves, the more accurate is the average value of the property. Similarly other particles are moved.

A common practice in Monte Carlo simulation is to select the atoms to move sequentially, i.e., in the order of the atom index rather than randomly. This cuts down on the amount of random number generation and is an equally valid method of generating the correctly weighted states (Hastings, 1970). The biggest drawback in using the Monte Carlo methods is the lengthy and expensive computational time.

Phase Inversion

The reversal of phases is a major instability in emulsions. The process by which the dispersed phase becomes the continuous phase, and vice versa, is known as phase inversion. The particles for one or other reason come in contact and flow together. Instead of separating, the dispersed phase occludes portions of the external phase, which thereupon becomes discontinuous, forms globules under the influence of the interfacial tension and appears as the new dispersed phase in the former internal phase, now the continuous phase.

Differing views exist in literature reasoning how and when inversion occurs. Inversion may occur when the volume fraction of the internal or dispersed phase exceeds a certain critical value (Lissant, 1987). Smith and Lim

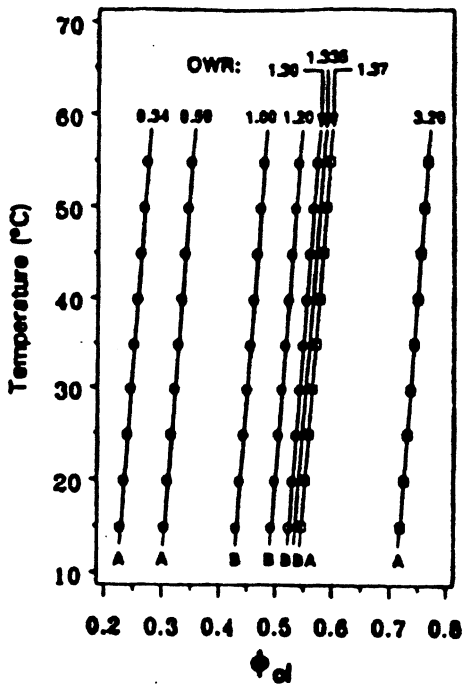

Figure 3. Temperature and Oil Phase Volume Fractions, and Experimental paths, for which the Emulsion Morphology remained Unchanged: Circles, O/W Morphology; Squares, W/O Emulsions. (Smith et al., 1991)

these two temperatures thus contradicting the PIT idea. The x-axis in figure 3 is the volume fraction of the dispersed oil phase and the y-axis, the temperature of the system. OWR is the oil to water ratios used by Smith et al. to find the emulsion morphology. The authors did not find any indication of inversion even when the temperature was changed in both directions from 20 °C below the PIT to 20 °C above the PIT.

The maximum volume fraction possible for an internal phase made up of uniform, incompressible spheres is 74%. Usually inversion occurs when the internal volume fraction exceeds some value reasonably close to 0.74. Other

factors have a bearing as well, of course, including the nature and concentration of emulsifiers and physical influences such as temperature or the application of mechanical shear. Bhatnagar (1920) conducted experiments using different volume ratios of oil and water phase with soaps to bring about inversion and found that trivalent electrolytes are more effective than bivalent electrolytes in bringing about inversion.

The effects of shear rate, temperature and oil concentration on the formation of oil-in-water emulsions using California crude were studied by Mao and Marsden (1977) as referred by Payne and Phillips (1985). Mao & Marsden noted that increases in temperature or oil concentration enhanced the conversion of oil-in-water emulsions to water-in-oil emulsions. Ross and Kornbrekke (1989) reported a new phenomenon that the morphology of an unstabilized liquid-liquid dispersion to be predicted by a statistical law. They defined the inversion point as the volume ratio, all other variables being constant, at which the probabilities of obtaining the two morphological types of dispersion are equal.

All the above science detailed in this chapter is used in the next chapter to develop an approach for the problem of phase inversion. The methodology includes the derivation for the maximum and minimum drop size and the Metropolis Monte Carlo method to determine the drop size distribution.

CHAPTER III

MODEL DEVELOPMENT

This chapter presents the methodology used to predict the inversion point in an emulsion. The system considered is a three-phase annular flow with a gas core and a two-phase annular liquid film at the walls such as would exist in a typical gas well. The liquid film is present as an emulsion with a dispersed phase present as droplets in the continuous phase. The determination of the distribution of drop sizes in the system is found using the Monte Carlo method. The stable drop size distribution is used to calculate the energy of the emulsion system. Drop size distributions are determined for both types of emulsion. The prediction of the point of emulsion inversion.is based on the energy levels of the emulsion types.

In particular this chapter includes, the physical model of the three phase annular system in the gas well; the derivation of the maximum and minimum drop diameters in the two-phase annular liquid film; determination of the distribution of drop sizes using the Monte Carlo method; and the prediction of the point of emulsion inversion.

Physical Model

This section explains the physical model of the three-phase system and the assumptions made in solving the problem of predicting the inversion point. The flow pattern for an annular flow in gas well is shown in Figure 4. The downhole gas well system can be visualized as follows:

a) Gas at high pressure and temperature flows upward at a high velocity with or without formation water.

b) The condensation of water may occur at some point in the well because of a decrease in temperature along the well.

c) Since the gas velocity is very high, the gas flows in the center and the condensed water and oil flows along the sides of the tube as an emulsion. This type of flow is known as annular three-phase flow. Other types of flow such as the slug flow also exist but were not considered. The dispersed phase could be either water or oil depending on the location along the well.

The following assumptions are made in solving the problem of predicting the conditions under which phase inversion will occur.

1. The dispersed phase droplets are spherical.
2. Surface active agents are assumed to have no effect on the drop breakup and drop coalescence.

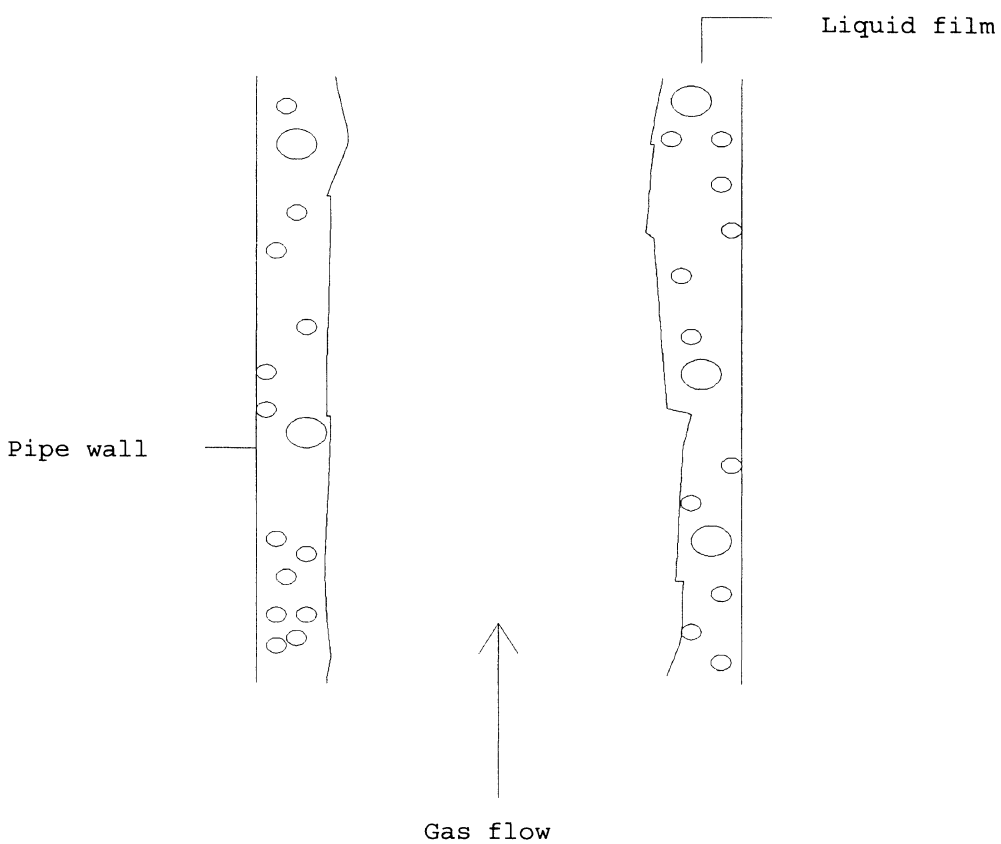

Figure 4. Schematic Diagram of Downhole Annular Two-Phase Gas/Liquid Flow

3. No inversion is possible when either phase is present in concentrations greater than 74 volume percent.

Determination of Drop Size

This section deals with the derivation of formulae for the calculation of the maximum and minimum diameters of the dispersed phase in the annular section. Levich (1962) derived the equations on the basis of the forces that are breaking and resisting the breakage of the drop.

At a certain value of the Reynolds number, steady laminar flow gives way to turbulent flow. Turbulent eddies are characterized by the size of the turbulent eddies. These distances are known as the scale of motion. The most rapid eddy motion has the largest scale of motion. The velocity, v′ of the most rapid eddy is

$$v' \approx \Delta U \qquad \text{(III-1)}$$

where ΔU is the change in the average velocity over a distance equal to the scale of an eddy of size *l*.

In the case of turbulent motion in a tube, the largest scale of turbulence eddies is equal to the diameter of the tube. Such large scale eddies are the main part of the kinetic energy of turbulent motion. The Reynolds number of a turbulent eddy is

$$\mathrm{Re} = \frac{\Delta U\, l}{\nu}. \qquad \text{(III-2)}$$

where Re is the Reynolds number; l is the size of the eddy and ν is the kinematic viscosity of eddy. Along with these large scale eddies there are also eddies of smaller scale, λ with lesser velocities, v_λ. Though the numbers of small eddies are high they contribute only a small part of the kinetic energy of the stream. In fluid motion with large scale eddies, i.e., with scale $\lambda \approx l$, viscous forces have no effect and such motion takes place without any dissipation of energy. But small scale eddies for which Reynolds number decrease with decreasing λ, are accompanied by energy dissipation.

The large scale eddies create a large quantity of small scale motion. The small scale motions release energy, which is transformed to heat. Thus the small scale eddies serve as a bridge by means of which the kinetic energy of large scale motion is converted to thermal energy. The conclusion is: although turbulent motion occurs at high Reynolds number, it is accompanied by a considerable amount of energy.

Considering the case of turbulent motion having a scale of $\lambda << l$, i.e.,. small scale turbulence at a distance from the solid walls, the characteristics of flow are determined. However, $\lambda >> \lambda_0$ where λ_0 is the scale at which the Reynolds number of motion is unity. The velocity v_λ, is the velocity of turbulence eddies in scale λ and is a function of density, ρ, scale, λ and the

constant ε, since these characterize the motion of the scale.

$$v_\lambda = \left(\frac{\varepsilon\lambda}{\rho}\right)^{\frac{1}{3}}. \qquad \text{(III-3)}$$

The energy ε can be determined from quantities characteristic of large scale turbulent motion, which includes the velocity, U, the scale of motion *l*, and the density of fluid, ρ. Thus,

$$\varepsilon = \frac{\rho \Delta U^3}{l}. \qquad \text{(III-4)}$$

using the above relation,

$$v_\lambda = \Delta U \left(\frac{\lambda}{l}\right)^{\frac{1}{3}}. \qquad \text{(III-5)}$$

Thus eddy velocity for motion of scale λ is smaller than the velocity of main flow by a factor $\left(\frac{\lambda}{l}\right)^{\frac{1}{3}}$.

The fragmentation of drops depends on the velocity changes from one point to another in a turbulent stream. The velocity of the liquid at the surface of the drop also varies from point to point. Thus different dynamic pressures will be exerted at different points on the surface of the drop. Under certain conditions, these will inevitably lead to the deformation of the drop.

If we assume that the difference in the densities of the drop and the medium is close, then the difference in

dynamic pressure exerted on opposite sides of a drop with a diameter 2a is

$$Q = K_f \rho \frac{v_1^2 - v_2^2}{2a}. \qquad \text{(III-6)}$$

where v_1 and v_2 are the velocities of the medium at points separated from each other by a distance 2a; Q is the dynamic pressure; and K_f is a constant. Levich assumed isotropic turbulence, i.e., the relative velocity is dependent on local energy per unit mass. For a change in eddy velocity, we have

$$v = \left(\frac{\varepsilon\lambda}{\rho}\right)^{\frac{1}{3}} = (\varepsilon_0\lambda)^{\frac{1}{3}}. \qquad \text{(III-7)}$$

where ε_0 is the energy dissipation per unit mass. After some arithmetic manipulations, the following equation results:

$$Q = \left(\frac{K_f v^2}{2}\right)\left(\frac{1}{\lambda_0}\right)^{\frac{8}{3}} (2a)^{\frac{2}{3}}. \qquad \text{(III-8)}$$

From a force balance on the droplet,

dynamic pressure $\approx$ capillary pressure.

$$\left(\frac{K_f \rho v^2}{2}\right)\left(\frac{1}{\lambda_0}\right)^{\frac{8}{3}} (2a)^{\frac{2}{3}} \approx \frac{\sigma}{a_{cr}}. \qquad \text{(III-9)}$$

which is solved for the critical radius as

$$a_{cr} \approx \left(\frac{\sigma}{K_f \rho v^2}\right)^{\frac{3}{5}} (\lambda_0)^{\frac{8}{5}}. \qquad \text{(III-10)}$$

Since the thickness of the liquid film is so small, the maximum diameter of the drop could be approximated by the thickness of the liquid film, δ.

$$d_{max} = \delta. \qquad \text{(III-11)}$$

Droplet fragmentation distant from the walls occurs at the critical diameter given by the equation (III-11).

Levich then examines the breakup of drops caused by turbulent eddies in the non-homogeneous turbulent flow near the walls of the tube. In this case, the flow velocity and the spatial velocity gradient vary from point to point over the tubes cross-section. The distribution of the average velocity of flow over a distance, y, can be written in the form

$$U = \left(\frac{v_0}{\sqrt{\alpha}}\right) \ln\left(\frac{y}{\delta_0}\right). \qquad \text{(III-12)}$$

where U is the average velocity; v_0 is the eddy velocity; δ_0 is a small distance from the wall; y is the distance in the perpendicular flow; and α is a constant. The difference in dynamic pressure exerted on the two sides of the drop is

$$Q = 6\rho v_0^2 \left\{ \left[\ln\left(\frac{y+2a}{\delta_0}\right)\right]^2 - \left[\ln\left(\frac{y}{\delta_0}\right)\right]^2 \right\}. \qquad \text{(III-13)}$$

Assuming a << y, and by expanding in a Taylor's series, we have

$$Q = \frac{25\rho v_0^2 a}{y} \ln\left(\frac{y}{\delta_0}\right). \qquad \text{(III-14)}$$

From the conditions of the force balance,

$$\frac{\sigma}{a_{cr}} \approx \frac{25\rho v_0^2 a_{cr}}{y} \ln\left(\frac{y}{\delta_0}\right). \qquad \text{(III-15)}$$

$$a_{cr} \approx \sqrt{\frac{\sigma}{25\rho v_0^2} \frac{y}{\ln\frac{y}{\delta_0}}}. \qquad \text{(III-16)}$$

The conclusion is, at small y, i.e., near the wall, the drops that develop are smaller than those far away from the wall. By replacing the characteristic velocity v_0, by the average velocity, U,

$$a_{cr} \approx \frac{1}{U}\sqrt{\frac{\sigma}{\rho}\left(\frac{y}{\ln\frac{y}{\delta_0}}\right)}. \qquad \text{(III-17)}$$

The size of the drop is found to be inversely proportional to the average velocity and decrease as the wall is approached. The smallest drop size will be found in the

wall region at the boundary of the viscous layer where

$$y \approx \delta_0 \approx \frac{\nu}{v_0}.$$

$$a_{cr} \approx \sqrt{\frac{\sigma\nu}{25\rho v_0^2}}. \qquad \text{(III-18)}$$

$$d_{min} \approx 2\sqrt{\frac{\sigma\nu}{25\rho v_0^2}}. \qquad \text{(III-19)}$$

Thus, in the course of drop fragmentation, a distribution of drop size is formed in the range determined using equations (III-11) and (III-19) which can be used for our work. No strong evidence exists to support the use of the above equations but the equations suit our work requirement over other models in predicting both the minimum and maximum drop size; accounting for the drop deformation; and assuming turbulent eddies as the cause for breakup of drops.

Distribution of Drop Size

A control volume was taken in the shape of a 0.5cm x 0.5cm x 0.5cm cube. The volume of water in the cube is found by

$$V_w = X_w\,(0.5\text{cm})^3. \qquad \text{(III-21)}$$

where V_w is the volume of the water in the control volume and X_w is the volume fraction of water. The initial total

number of dispersed phase droplets in the cube is calculated by dividing the volume of water in the cube by the volume of a single drop. All the droplets are initially assumed to be of the same minimum diameter, D_{min}.

$$N = \frac{V_w}{\frac{\pi}{6} D_{min}^3}. \qquad \text{(III-22)}$$

where N is the total number of drops in the cube.

The Metropolis Monte Carlo method is now used to determine the drop size distribution. The steps involved in arriving at the drop size distribution can be listed as follows:

1) The N number of drops of the dispersed phase are placed uniformly in a Face Centered Cubic packing configuration.

2) If the volume fraction of oil is less than 0.26 corrosion is predicted because water will undoubtedly wet the pipe wall.

3) The energy of the initial configuration is calculated.

$$E_1 = f \text{ (drop configuration)}.$$

$$\text{Energy / drop} = \gamma A = \gamma \pi d^2. \qquad \text{(III-23)}$$

where γ is the interfacial tension between water and oil and A is the surface area of the drop.

$$\text{Total energy} = \gamma\pi\sum_{i=1}^{N} d^2 . \qquad \text{(III-24)}$$

4) A random Monte Carlo move which is the change in position of a drop in all three directions is made. Any number of drops between 0 and N could be moved at the same time. The present work moved one drop at a time. The equations for performing the move of a drop is given by

$$X_i^{new} = X_i + (0.5-\xi_1)\Delta q_i . \qquad \text{(III-25)}$$

$$Y_i^{new} = Y_i + (0.5-\xi_2)\Delta q_i . \qquad \text{(III-26)}$$

$$Z_i^{new} = Z_i + (0.5-\xi_3)\Delta q_i . \qquad \text{(III-27)}$$

where X_i, Y_i, Z_i are the coordinates of a drop before the move is made; X_i^{new}, Y_i^{new}, Z_i^{new} are the new positions of the drop after the move is made; ξ_1, ξ_2, ξ_3 are random numbers uniformly distributed between 0 and 1; and Δq_i is a number between 0 and 1 found by trial and error technique. The magnitude of Δq_i is selected such that approximately half of the moves performed are accepted.

$$\frac{N_{accept}}{N_{reject}} \approx 1 . \qquad \text{(III-28)}$$

5) If the distance between the new position of the drop to its nearest neighbor is less than a critical distance, R_{crit}, then the drops are assumed to combine together to form a bigger drop. Let R_{ij} be the distance between the drop and its neighbor after the move. If $R_{ij} < R_{crit}$, then the drops coalesce together to form a drop of total volume

$$\text{Totvol} = \frac{4}{3}\pi\left(r_i^3 + r_j^3\right). \qquad \text{(III-29)}$$

where r_i is the drop moved randomly and r_j is the drop nearest to r_i. Thus the diameter of the new drop would be

$$d^{new} = \sqrt[3]{d_i^3 + d_j^3}\,. \qquad \text{(III-30)}$$

If none of the neighboring drops are within the critical distance to the moved drop, the drop moved is placed in its new position and another drop is chosen to perform the Monte Carlo move.

6) If the drops combine the newly formed bigger drop is checked with the size of the maximum diameter to decide whether to breakup the drop into two droplets or remain as a single stable droplet. The probability of drop breakup depends on the strength of the flow field and the size of the drops, hence:

$$P = f(\dot{\gamma}, d). \qquad \text{(III-31)}$$

where P is the probability of breakup, $\dot{\gamma}$ is the second invariant of the rate of strain tensor and d is the diameter of the drop. The functional forms of the dependency of the probability of breakup on d and $\dot{\gamma}$ were assumed to be separable.

$$P = g(d)\, h(\dot{\gamma}). \qquad \text{(III-32)}$$

An empirical dimensionless equation proposed in the present work based on an exponential distribution, for the breakup due to the size of the drops, was introduced.

$$g(d) = \exp - \left(\frac{4.6(d_{max} - d)}{d_{max} - d_{min}} \right). \qquad \text{(III-33)}$$

According to the above expression the probability of breakup of a drop due to its size would be between 0.01 and 1. The value of 4.6 that appears in equation (III-33) was chosen such that the breakup of a drop of minimum size would be 0.01.

The other factor that affects the probability of breakup is the strength of the flow field. In the present work, values of the strength of the flow field were assumed between 0 and 1. The exact value of the strength of the flow field is not known at this point of research. But the following direction can be taken to calculate the strength of the flow field. If pure shear flow is assumed and from Newton's law of viscosity,

$$\dot{\gamma}_{liquid} = \frac{\tau}{\mu_{liquid}}. \qquad \text{(III-34)}$$

where $\dot{\gamma}_{liquid}$ is the second invariant of the rate of strain tensor, τ is the shear stress and μ_{liquid} is the viscosity of the liquid in the film. Using the above relation, the second invariant of both emulsion types present in the liquid film can be calculated.

The probabilities of breakup of all drops in the system are calculated. A random number is generated between 0 and 1 and is compared with the probability of breakup of a drop. If the value of the random number is less than the

probability, the drop breaks up into two droplets. The next random number is generated and checked with another drop to decide the breakup. The procedure is continued until all drops in the system is checked.

7) A new configuration with a different number of varying diameters is formed. The energy of this new configuration is calculated as before

$$E_2 = f \text{ (drop configuration after move)}.$$

The change in the energy between the new and the old configuration is calculated by

$$\Delta E = E_2 - E_1. \qquad \text{(III-35)}$$

8) The Boltzmann factor, $\exp(-\Delta E/RT)$ is calculated where R is the ideal gas law constant and T is the temperature of the section being considered. A random number between 0 and 1 is compared with the Boltzmann factor. If the random number is less than the Boltzmann factor, the Monte Carlo move made on the drop is accepted. If the random number is greater than the Boltzmann factor, the move is rejected and another attempt to move from the original configuration is made, i.e.,

$$\text{If} \quad \xi < \exp-\left(\frac{\Delta E}{RT}\right) \text{ accept move,} \qquad \text{(III-36)}$$

$$\xi > \exp-\left(\frac{\Delta E}{RT}\right) \text{ reject move.} \qquad \text{(III-37)}$$

9) If the moves are accepted, the new configuration becomes the original and a Monte Carlo move is again made.

These steps are repeated until the termination criterion is satisfied. The first, second and the third moments of the drop diameters are calculated initially before performing any moves as

$$\langle D \rangle = \frac{1}{N}\sum_{i=1}^{N} D . \qquad \text{(III-38)}$$

$$\langle D^2 \rangle = \frac{1}{N}\sum_{i=1}^{N} D^2 . \qquad \text{(III-39)}$$

$$\langle D^3 \rangle = \frac{1}{N}\sum_{i=1}^{N} D^3 . \qquad \text{(III-40)}$$

The moments are again calculated after 1000 moves. The percentage difference between the moments calculated initially and after 1000 moves is calculated as

$$\% = \frac{\langle D \rangle_{M=0} - \langle D \rangle_{M=1000}}{\langle D \rangle_{M=1000}} \times 100 . \qquad \text{(III-41)}$$

If this percentage is less than any allowable limit, say, 5% then the moments are said to be constant over the moves. The same is done for the second and third moments. If all the three conditions are not satisfied, the next 1000 moves are made. Comparison is made between the new set of calculated moments and the previous one.

$$\% = \frac{\langle D \rangle_{M=1000} - \langle D \rangle_{M=2000}}{\langle D \rangle_{M=2000}} \times 100 . \qquad \text{(III-42)}$$

Thus the Monte Carlo moves are made until the termination condition is satisfied resulting in different number of total drops of varying diameters ranging between D_{min} and

D_{max}. This is the required drop size distribution. In the present work the convergence was assumed to have occurred after 100,000 moves.

Prediction of the Inversion

The prediction of the inversion point depends on the energy levels of the system with water dispersed and oil dispersed. From the last step of the Monte Carlo method, the energy of the final configuration is calculated. Now the dispersed phase is assumed to be the continuous phase and vice versa. The Monte Carlo technique is applied to this system and the energy of the final configuration of this system is found. The energies of both the configurations are compared. The configuration with the lowest energy is the more favored emulsion.

If the stable emulsion is the oil-in-water emulsion then water wets the tube wall and corrosion is assumed to begin. If the stable emulsion is the water-in-oil emulsion, then water does not wet the pipe wall and corrosion is assumed not to occur.

Numerical Aspects of the Model

The total number of drops was about 2760 drops for a minimum drop diameter of 0.04 cm. The drops were placed uniformly in a cube lattice before the simulation began.

This required the solution of a cubic equation. The total number of drops are

$$N = NDR^3 + 6(NDR-1)^2 + 3(NDR-2)(NDR-1)^2 . \quad \text{(III-43)}$$

where NDR is the number of drops along each side of the cube in a Face centered cubic packing. The above cubic equation after simplifying is

$$4NDR^3 - 6NDR^2 + 3NDR - N = 0 \quad \text{(III-44)}$$

The above equation was solved using the Bisection method. This method was chosen because this method did not require an initial guess. The upper and the lower limits were known. Hastings method was followed for making the Monte Carlo moves by moving the drops sequentially by its index.

Summary

The method of solution is summarized in the form of the flowsheets below. The overall computational strategy to predict the location of emulsion phase inversion is given in Figure 5. To start with, a dispersed phase concentration of 26% of water is assumed. The maximum and minimum drop diameters can be calculated using the equation derived. The present work assumed the value of the minimum and maximum diameter as 0.04 cm and 0.08 cm, respectively. The Monte Carlo method is employed to determine the drop size distribution of the water droplets in oil. The oil phase is then assumed to be the dispersed phase and the distribution

the rate of strain tensor, which in case of pure shear flow is the shear rate. The drops break up into two equal sized droplets if the probability of breakup is greater than a randomly generated probability.

The drop size is constrained by maximum and minimum diameter values. When coalescence and breakup have been considered for each droplet, an energy for the new drop size distribution is calculated. The entire process is repeated until the drop size distribution and system energy becomes independent of the cycles.

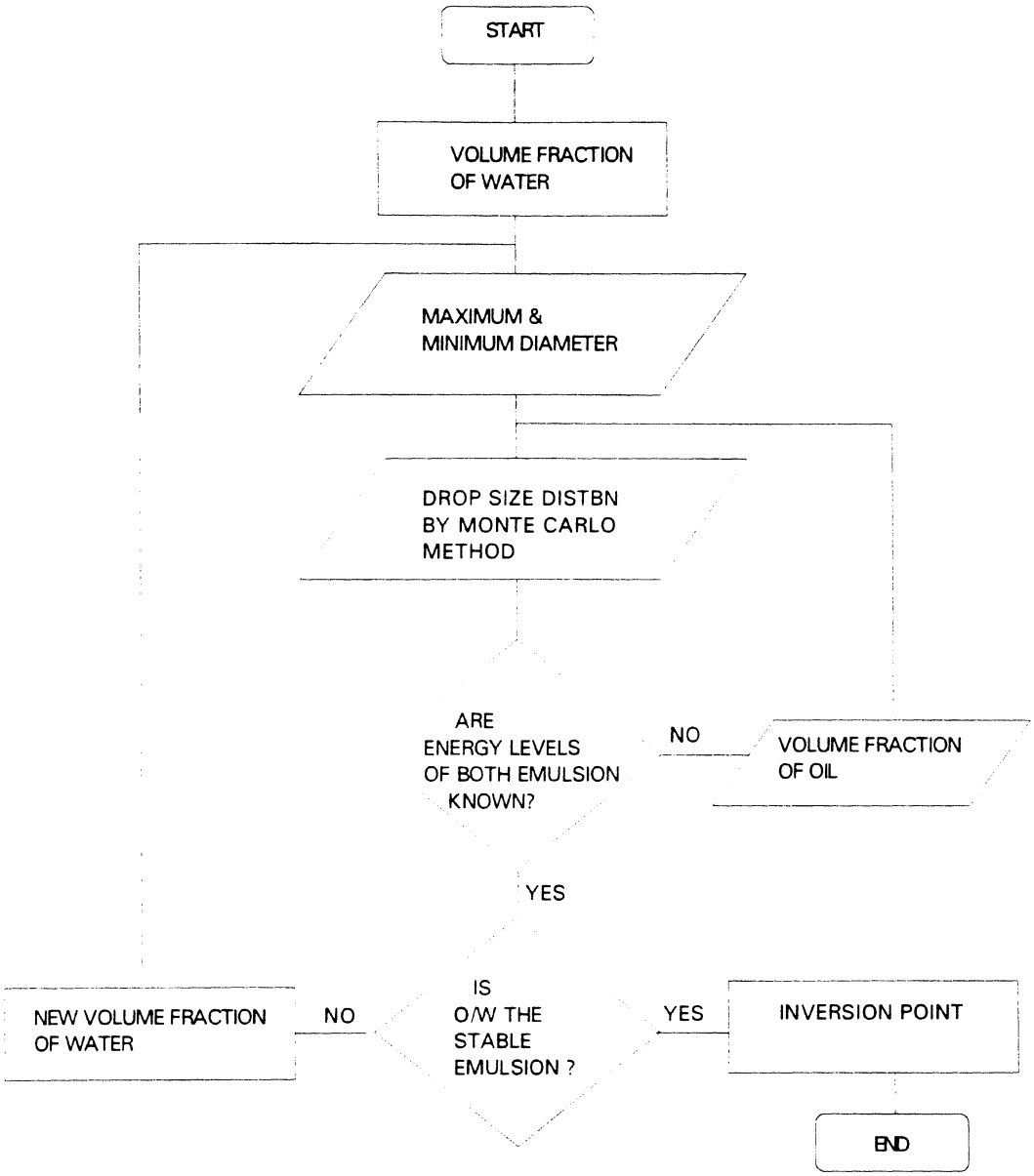

Figure 5. General Algorithm Flowsheet to Predict the Inversion Point.

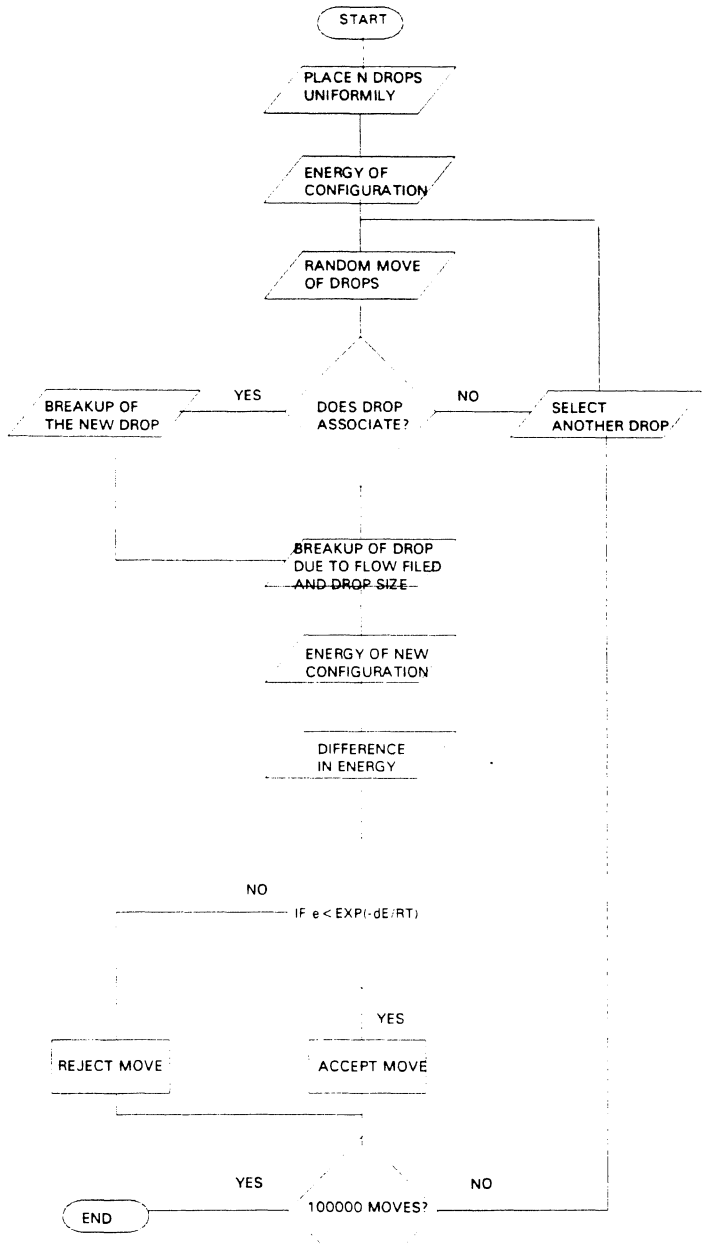

Figure 6. Monte Carlo Method Flowsheet to Determine the Drop Size Distribution of the Emulsion.

CHAPTER IV

RESULTS AND DISCUSSION

This chapter presents the results of the Monte Carlo simulation for three cases to demonstrate and discuss the model. A "normal" case and two extreme cases, for which the solutions were known are presented to illustrate the model. The model validation also included the testing of the mass balance in the system.

Table 1. Input Data for Two Extreme and a Normal Case with respect to the Strength of the Flow Field

Cases	Case 1	Case 2	Case 3
Strength of the Flow field	0	1	10^{-14}
Volume fraction of Water	0.58	0.49	0.50
Minimum Diameter	0.04 cm	0.04 cm	0.04 cm
Maximum Diameter	0.08 cm	0.08 cm	0.08 cm
Number of Moves	100000	100000	100000

A confidence in the model is developed in the reader by performing the simulation for known case results and comparing both the results. Table 1 shows the input data for the two extreme cases and a normal case with respect to the strength of the flow field. The probability of breakup of drops is equal to the product of the normalized function of the strength of the flow field and a normalized function of the drop size. In the two extreme cases, the function of the strength of the flow field is equal to one (strong strength of flow field) and zero (weak strength of flow field). The normal case is assumed a strength of flow field such that the probability of breakup and coalescence of drops are equal.

The input quantities for the Case 1 are shown in the Table 1. This case can be compared to the emulsion system with no external source of energy. Under these conditions no drop breakup, and only drop coalescence is possible. The above experiment would result in a stable system with equisized dispersed drops. The Monte Carlo simulation was performed on this system to confirm the above science. A dispersed phase concentration of 58% of water was inputted into the code and very few drop breakup was observed due to the weak strength of the flow field. The run printed out the presence of few drops of maximum size at the end of the Monte Carlo simulation. The following plot explains the above results.

Figure 7 shows the histogram for the water droplets dispersed in Case 1. The histogram was drawn by grouping all the drops that resulted from the model by size. The horizontal line in the histogram is interpreted as the number of droplets between drop sizes corresponding to the ends of the line. In figure 7, 25 droplet of diameters between 0.065 cm & 0.07 cm, and 350 drops between 0.07 cm & 0.075 cm are present. Due to the weak strength of flow field, the drops broke up rarely resulting mostly in drops coalescence and very few breakups. The drop diameters are seen to be skewed more to the maximum diameter because of many drop coalescence and few drop breakups.

The volume of the dispersed phase was also checked time after time to see if the mass was conserved during the simulation. The volume of the system was calculated from the initial input of the volume fraction of the dispersed phase at the beginning of the simulation. For every 100 drop breakup and coalescence, the volume of the system was calculated. The mass was conserved at all times till the end of the simulation. The initial volume and the final volume of the dispersed phase for Case 1 are shown below thus satisfying the mass balance of the system.

initial volume	0.07244 cm^3
final volume	0.07244 cm^3

The second case can be compared to an emulsion system with an external source of energy. Under these conditions,

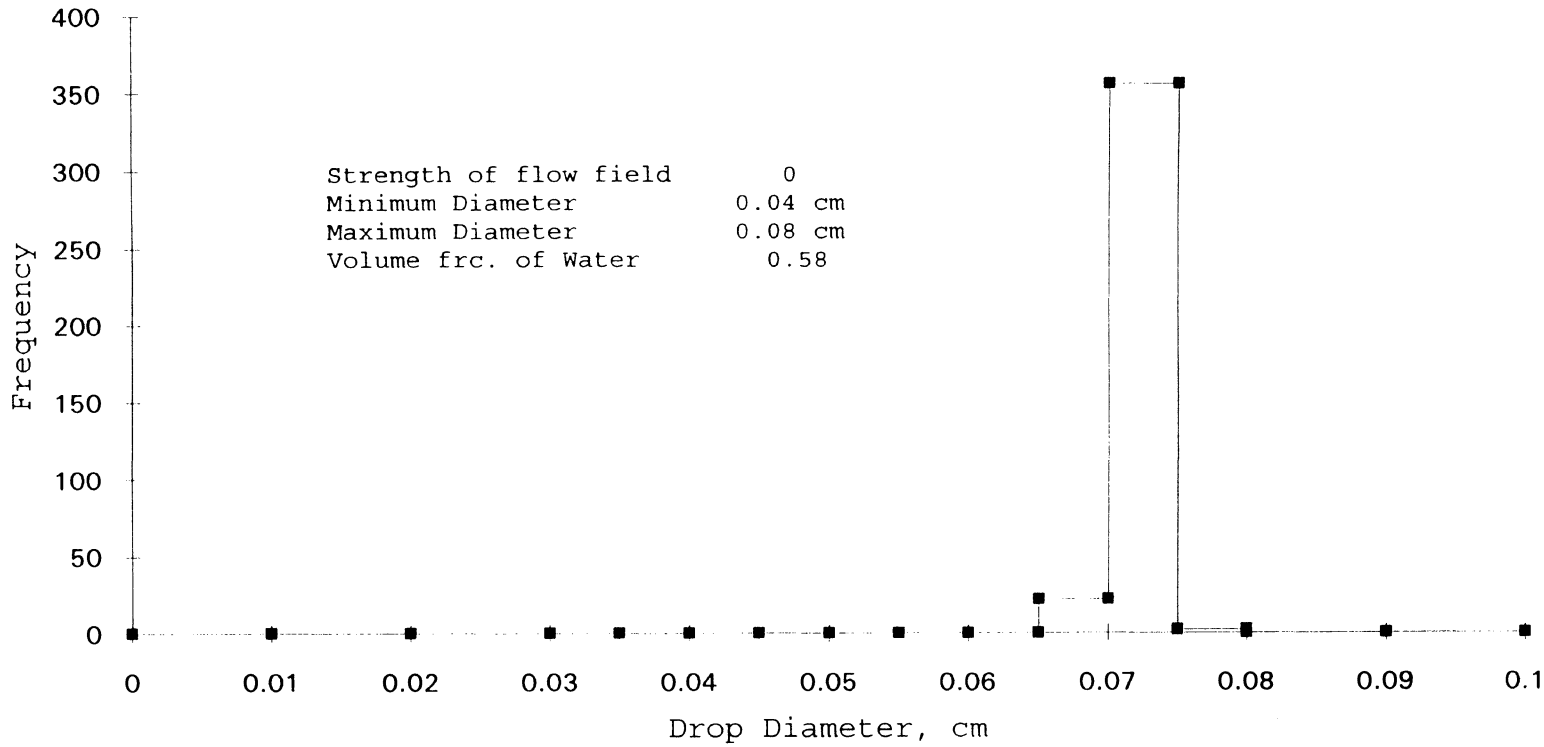

Figure 7. Histogram of Drop Size Distribution of Water Droplets (case 1)

no drop coalescence is possible, and the stable emulsion system would result in drops of minimum size. The Monte Carlo simulation was performed for the second case and the following plot of the histogram resulted from the run. Figure 8 presents the histogram for the water droplets dispersed in oil for a volume percentage of 49% of water. The histogram is interpreted the same way as the previous figure. Due to the very high strength of the flow field, the probability of breakup was high and the Monte Carlo method ended in a drop size distribution with most of the drops near the minimum droplet size. The mass balance was also checked for this case and the mass of the dispersed phase was conserved at the end of the run. In both of the above cases, the results for the drop size distribution were as would be expected from an emulsion system with and without external source, thus demonstrating the validity of the model.

In the third normal case, the strength of the flow field as represented by the second invariant of the rate of strain tensor was assumed to be 10^{-20}. Water was initially presumed to be the dispersed phase and the Monte Carlo simulation was performed to determine the drop size distribution. Then oil was taken to be the dispersed phase and Monte Carlo method was again used. Plots of the histogram of the drop size distribution are shown in figures 9 and 10.

Figure 9 and Figure 10 presents the histograms of the

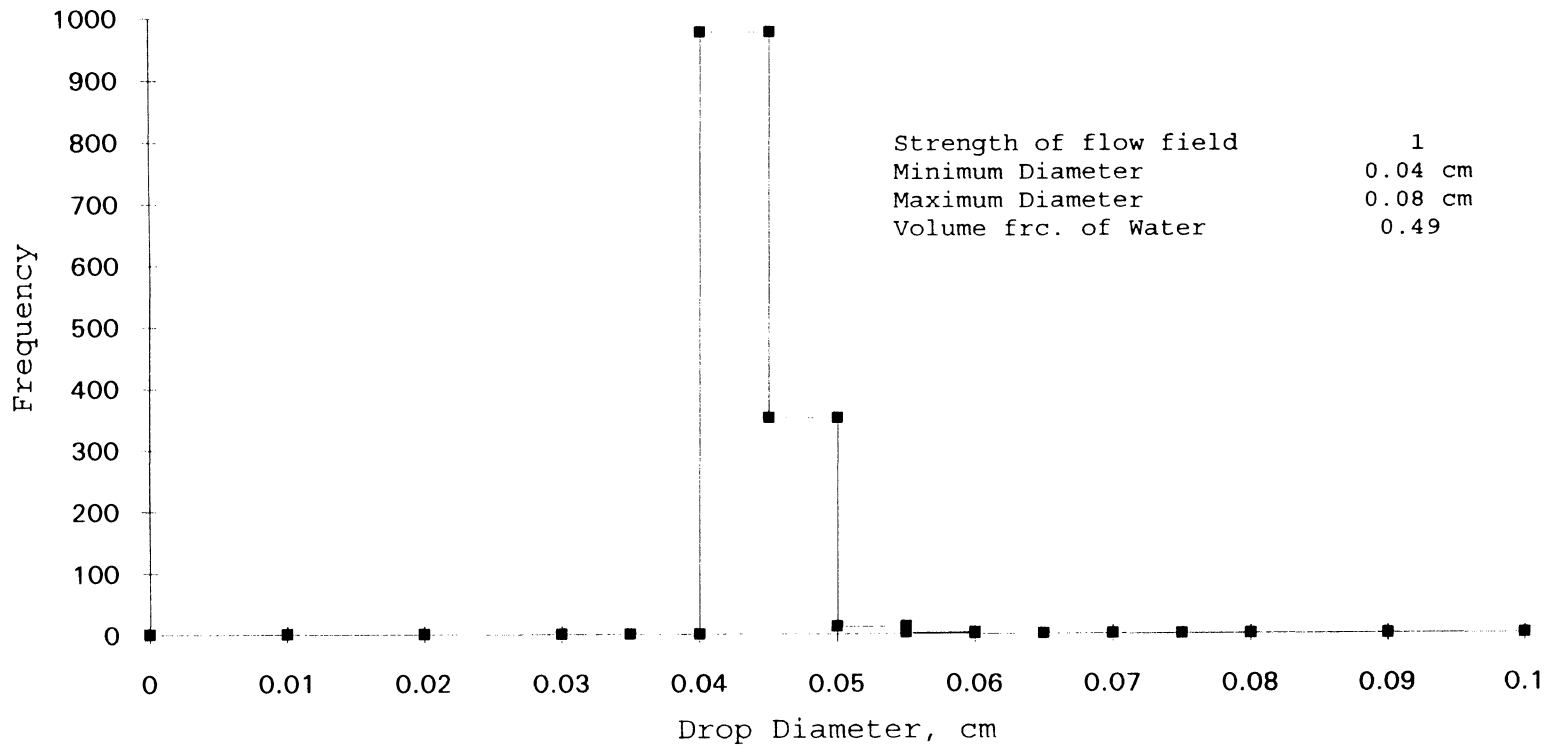

Figure 8. Histogram of Drop Size Distribution of Water Droplets (case 2)

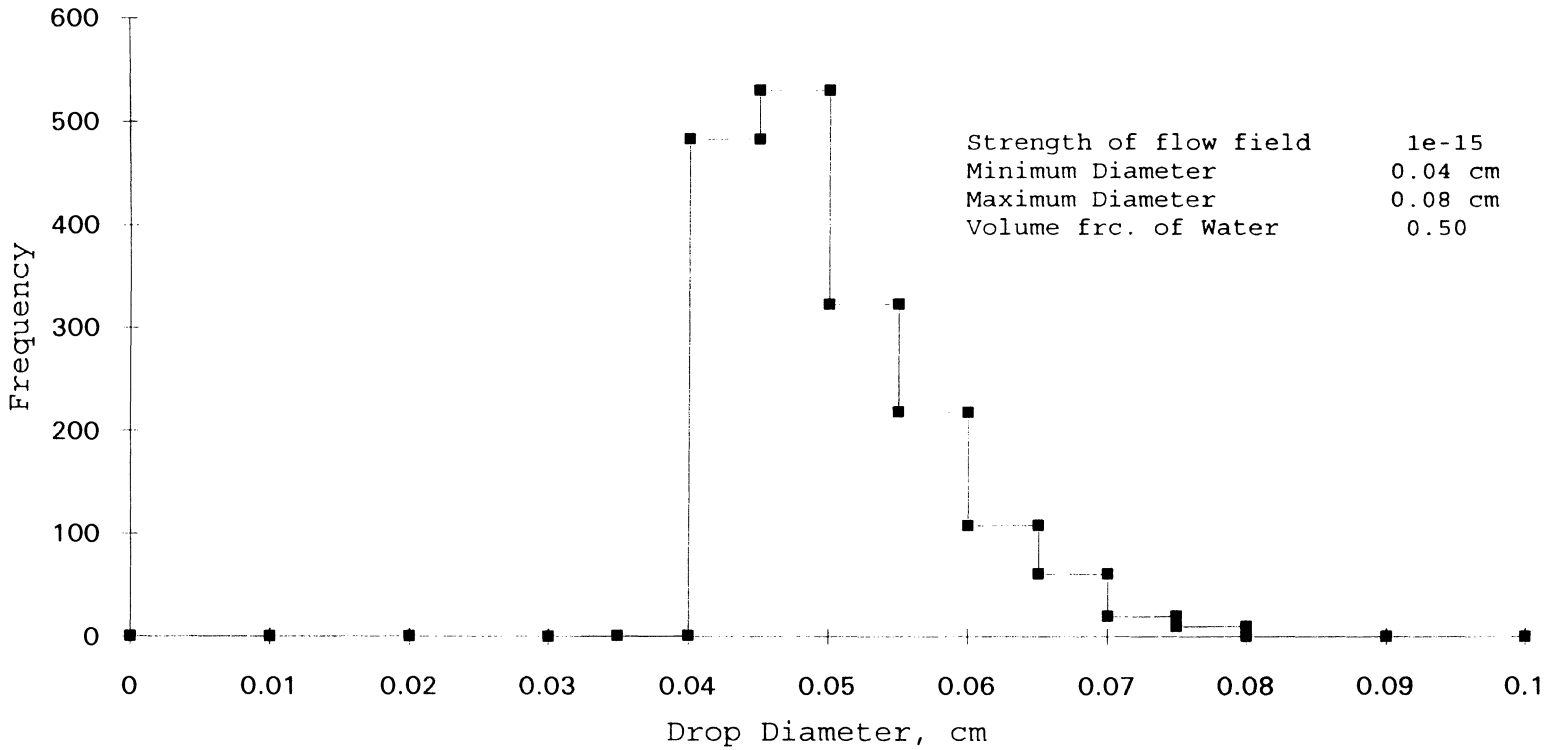

Figure 10. Histogram of Drop Size Distribution of Oil Droplets (case 3)

drop size distribution for the water droplets and oil droplets respectively. The histograms are in the form of an inverted bell. The drops are seen to be distributed over the whole interval between the maximum and minimum size. The peak of the histogram was observed to be skewed towards the minimum diameter relating the asymmetry of the log normal distribution. The shape of the histograms agreed very well to the log normal behavior of emulsions as proposed by researchers from experimental and empirical techniques (Clay 1940, Schwarz & Bezemer 1956, Scott et al. 1958).

A few more cases were run to illustrate the effect of the strength of the flow field on the drop size distribution of the dispersed phase. The strengths of the flow field were varied between 0(weak) and 1(strong). Histograms were drawn for all cases and figure 11 shows the distribution of all the cases in one plot. At strong strength of flow field, the drop size distribution was skewed to the minimum diameter of the drops. As the strength decreased, the distribution was seen to move towards the larger diameters. When the strength of the flow field was very weak, the distribution was skewed most to the maximum drop diameters. The peaks of the distribution were also seen to follow a pattern. The peaks decreased with decrease in the strength of the flow field till about a point where the peak starts to increase with decrease in strength of the field. This point could be called as the transition between the strong

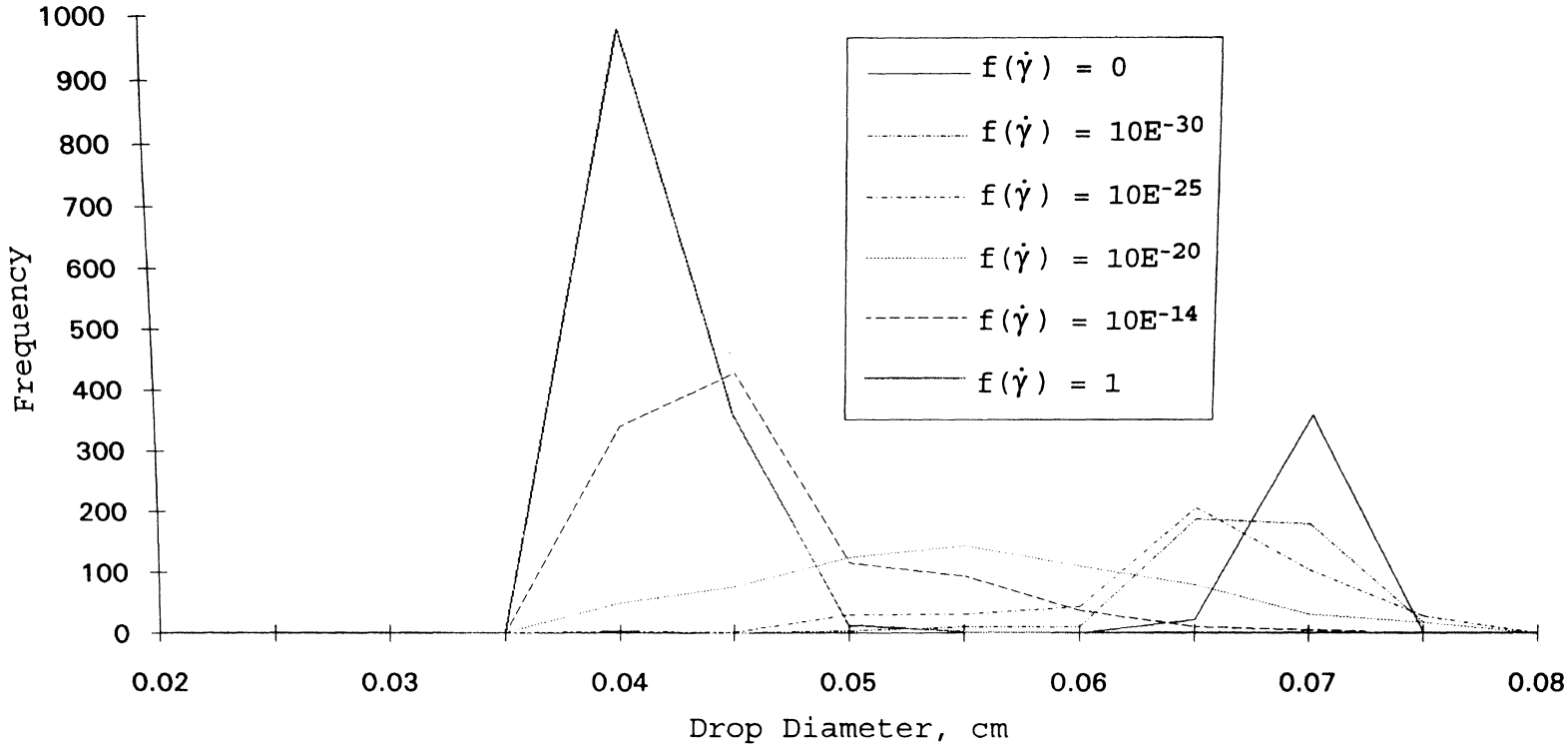

Figure 11. Drop Size Distribution as a Function of the Second Invariant of Water-in-Oil Emulsion

and weak strengths of flow fields. Thus from figure 11, the drop size distribution varies with the strength of the flow field.

The energy of the system demonstrates some reasonable behavior leading to a reasonable prediction of inversion point. Figures 12 to 15 shows the plots of the surface energy as a function of the number of Monte Carlo moves.

Figure 12 presents the surface energy vs. number of moves plot when the strength of flow field is weak. The energy reached a flat minimum implying either the non-occurrence of drop breakup and coalescence, or equal rates of drop breakup and coalescence. This type of energy behavior is seen in the simple emulsion system with no external source of energy, discussed in the beginning paragraph of this chapter. Figure 13 presents the surface energy against the number of moves graph for case 2. In figure 13, the surface energy approaches to reach a flat minimum with an increase in the number of moves. Due to the strong strength of the flow field, drops coalesce all the time and drop breakup is rarely seen. The fluctuation in the energy values is small because more new surface area is created than being destroyed. This behavior can be observed in an emulsion system with external source of energy.

Figure 14 and Figure 15 represent the variation of the surface energy with respect to the number of moves for water dispersed and oil dispersed emulsion system. In both of these figures, the surface energy was seen to either

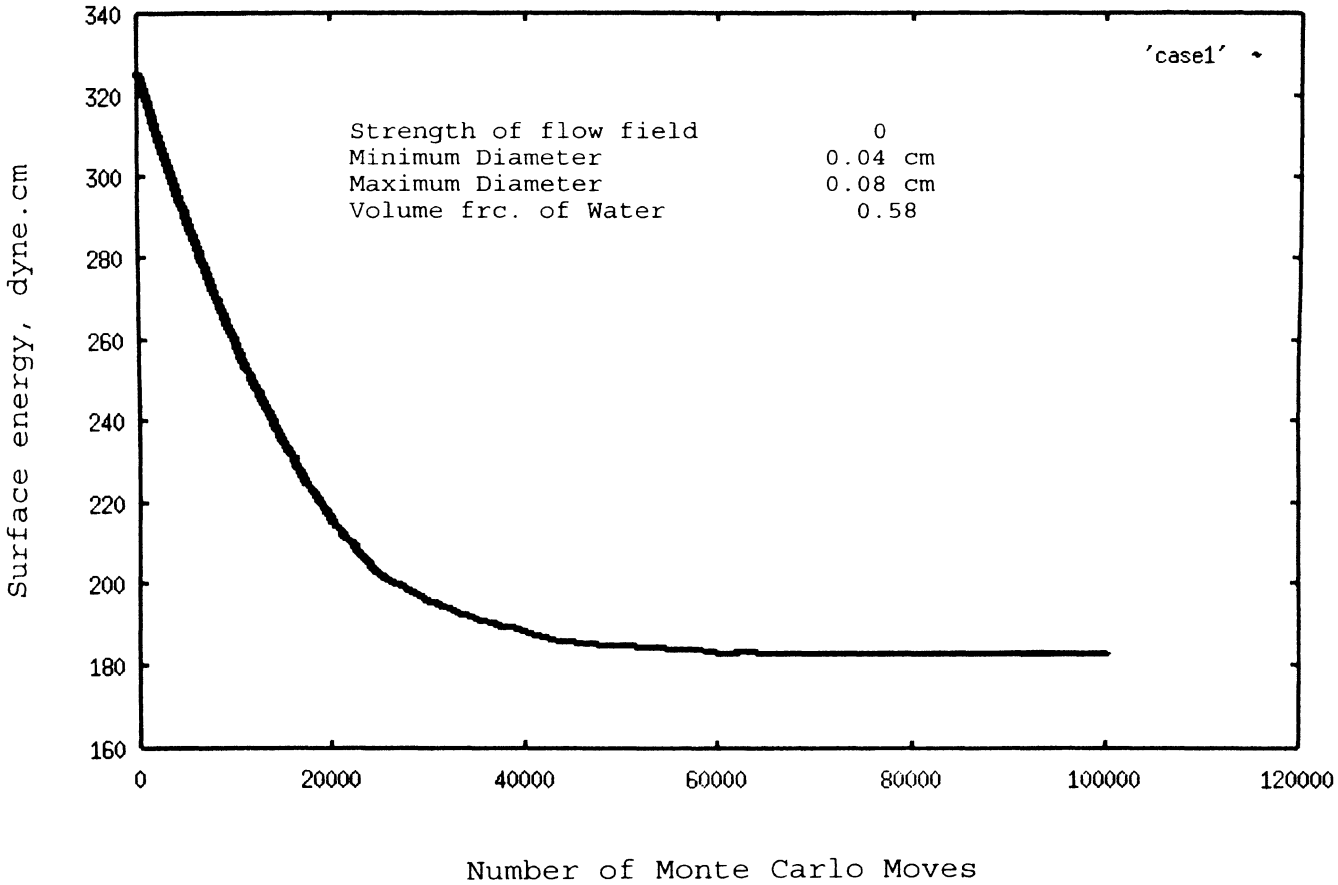

Figure 12. Surface Energy as a Function of Number of Monte Carlo Moves for $f(\dot{\gamma}_{w/o}) = 0$ and Water Dispersed in Oil.

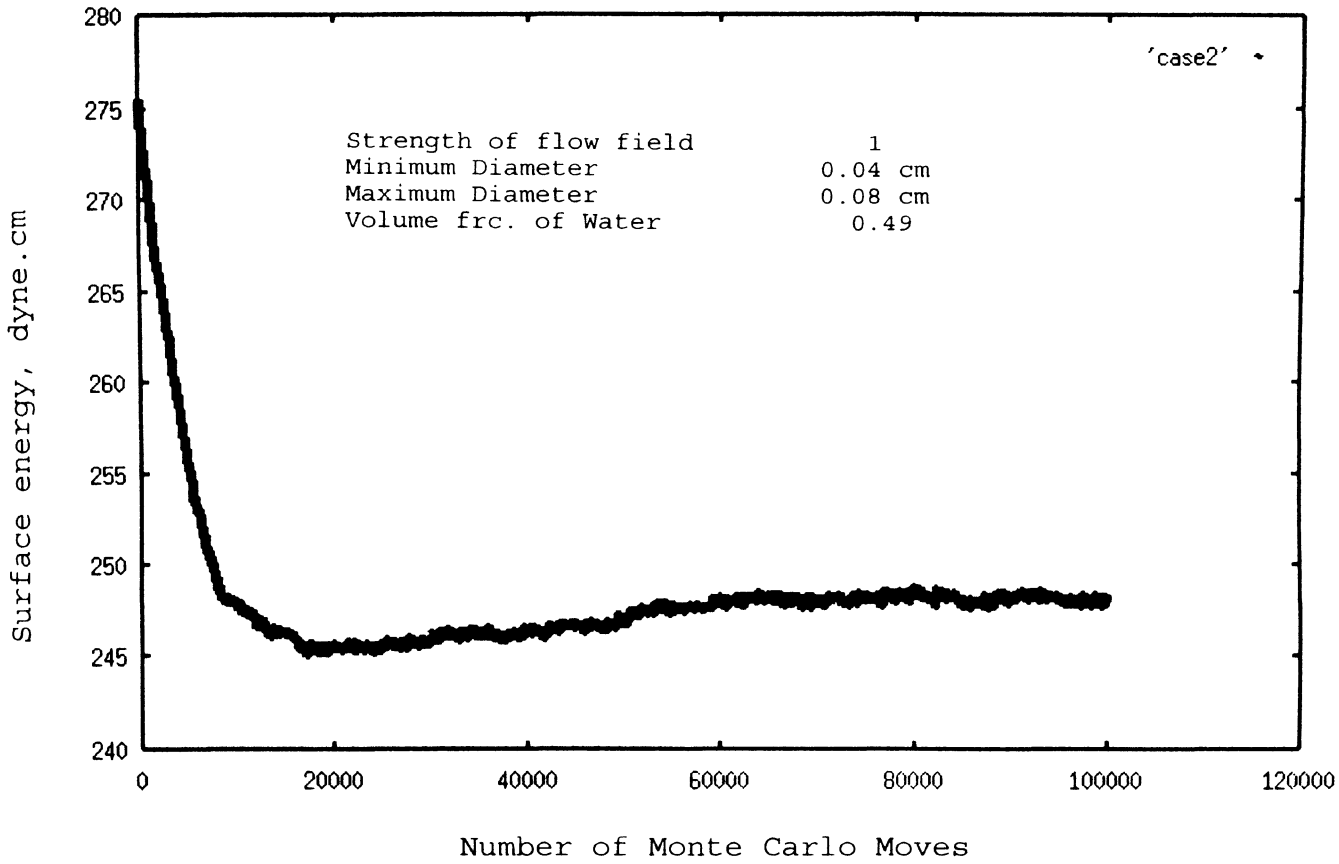

Figure 13. Surface Energy as a Function of Number of Monte Carlo Moves for $f(\dot{\gamma}_{w/o}) = 1$ and Water Dispersed in Oil.

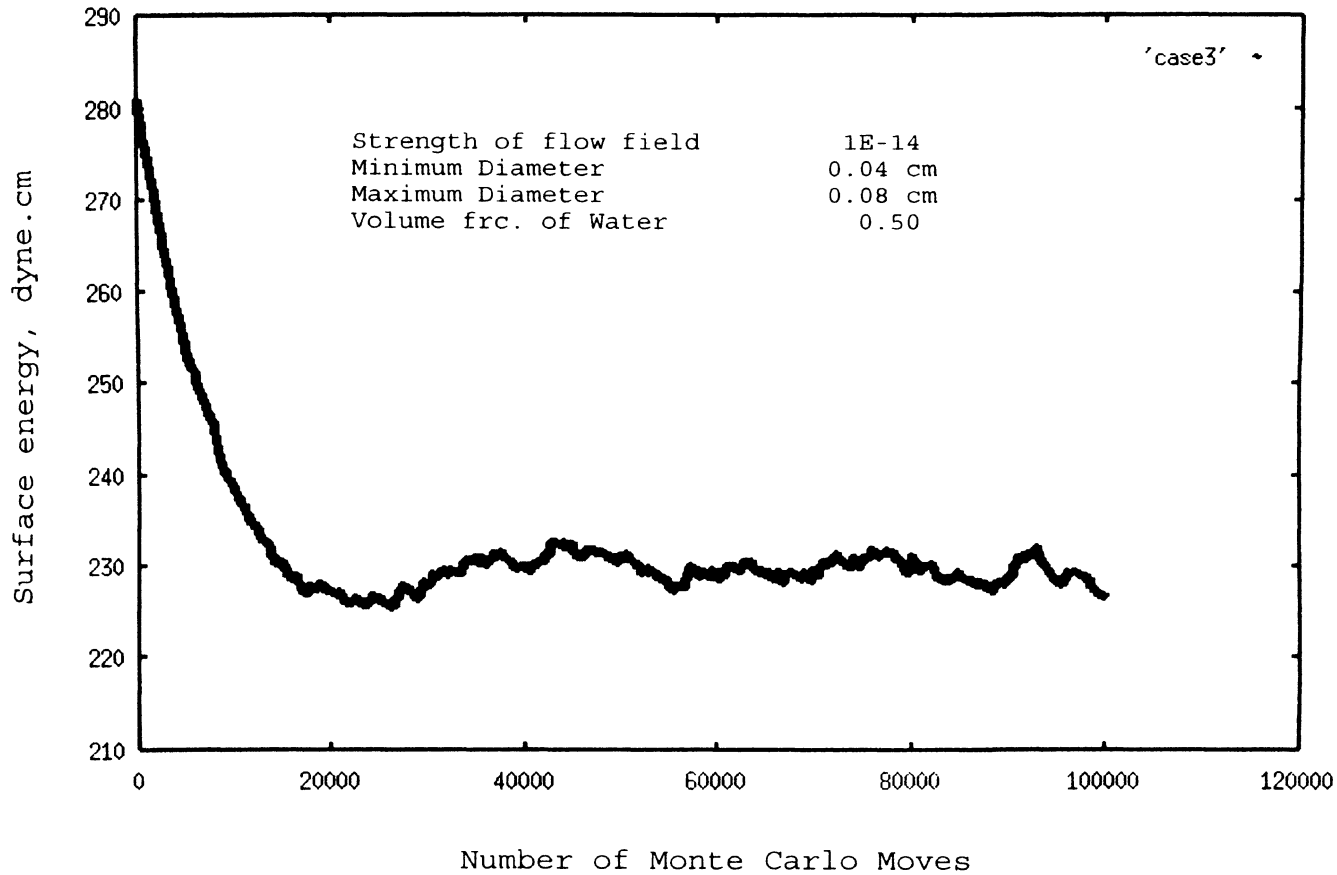

Figure 14. Surface Energy as a Function of Number of Monte Carlo Moves for $f(\dot{\gamma}_{w/o}) = 1x10^{14}$ and Water Dispersed in Oil.

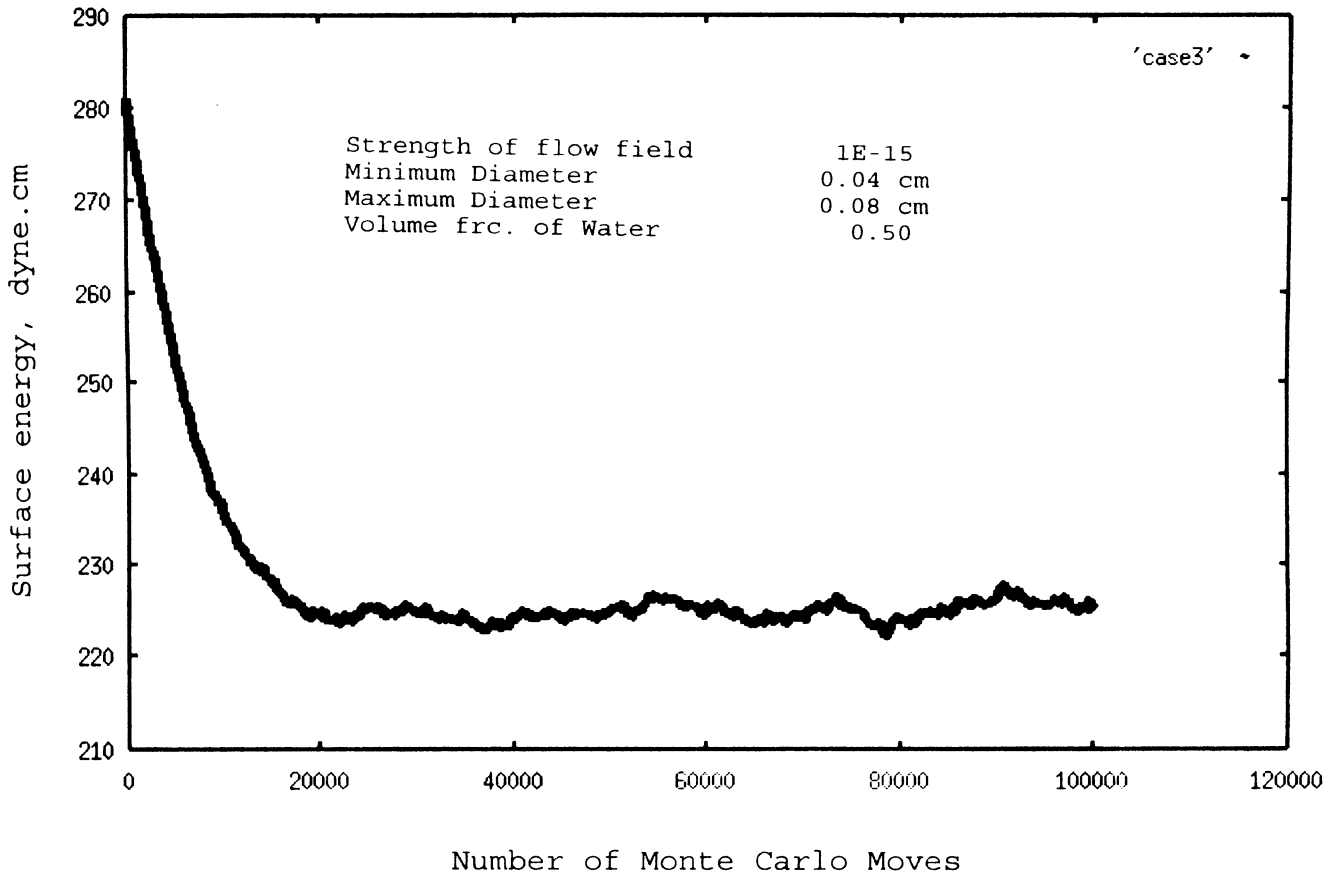

Figure 15. Surface Energy as a Function of Number of Monte Carlo Moves for $f(\dot{\gamma}_{o/w}) = 1x10^{-15}$ and Oil Dispersed in Water.

decrease or increase with an increase in the number of Monte Carlo moves. The fluctuation in the energy was due to the formation of new surface area and destruction of the surface area of the droplets. On the whole, the surface energy was noticed to decrease with the number of moves to a minimum energy level. At convergence the surface energy did not remain constant at a particular value. As the Monte Carlo moves increased, an increase and decrease in the surface energy was still seen and could be attributed to the random nature of the Monte Carlo numerical method.

Inversion points were predicted based on the energy levels of the emulsion system. The energy was calculated for the emulsion system assuming water as dispersed and oil as dispersed phases. On the basis of the energy levels, the more favorable emulsion type and hence the drop size distribution was determined. The procedure was repeated for, increasing volume fraction of the dispersed phase, to find the change in the stability of the emulsion type, and hence to predict the inversion point.

In all the above cases, the prediction of the inversion point depended on the difference in the values of the function of the second invariant between the two emulsion types. No idea of the relationship between the value of the second invariant and the strength of the flow field is known at this point of research. Hence the strengths of the flow field were assumed in all the cases considered. If the difference in the strength of the flow field for both water-

in-oil and oil-in-water emulsion is very small or the same, the inversion always occurred at 50% volume of water or oil. Figure 16 shows the phase inversion map if the second invariant of both the emulsion types are the same. The inversion was seen to occur always around 50%.

As the difference between the second invariants increased, the inversion point either increased or decreased. The inversion point was predicted in terms of the volume fraction of water. A plot between the strength of the flow field for water-in-oil emulsion and the volume fraction of water is presented in Figure 17. In all the cases represented by filled squares in this plot, the second invariant of the oil-in-water emulsion was 10^{-15} and that of the water-in-oil emulsion was varied between 0 and 1. The filled diamonds represent inversion points when the second invariant of the oil-in-water emulsion was 10^{-1} and the blank squares, when the second invariant of oil-in-water emulsion was 10^{-30}. It is obvious from this plot that the inversion point depends on the value of both the second invariants and the difference between the function of second invariants of emulsion types.

The value of the second invariant for both water-in-oil and oil-in-water emulsion is different. The value of the second invariant was calculated from the relation given by equation (III-34) for water-in oil and oil-in-water emulsion. The approximate value for the shear stress can be

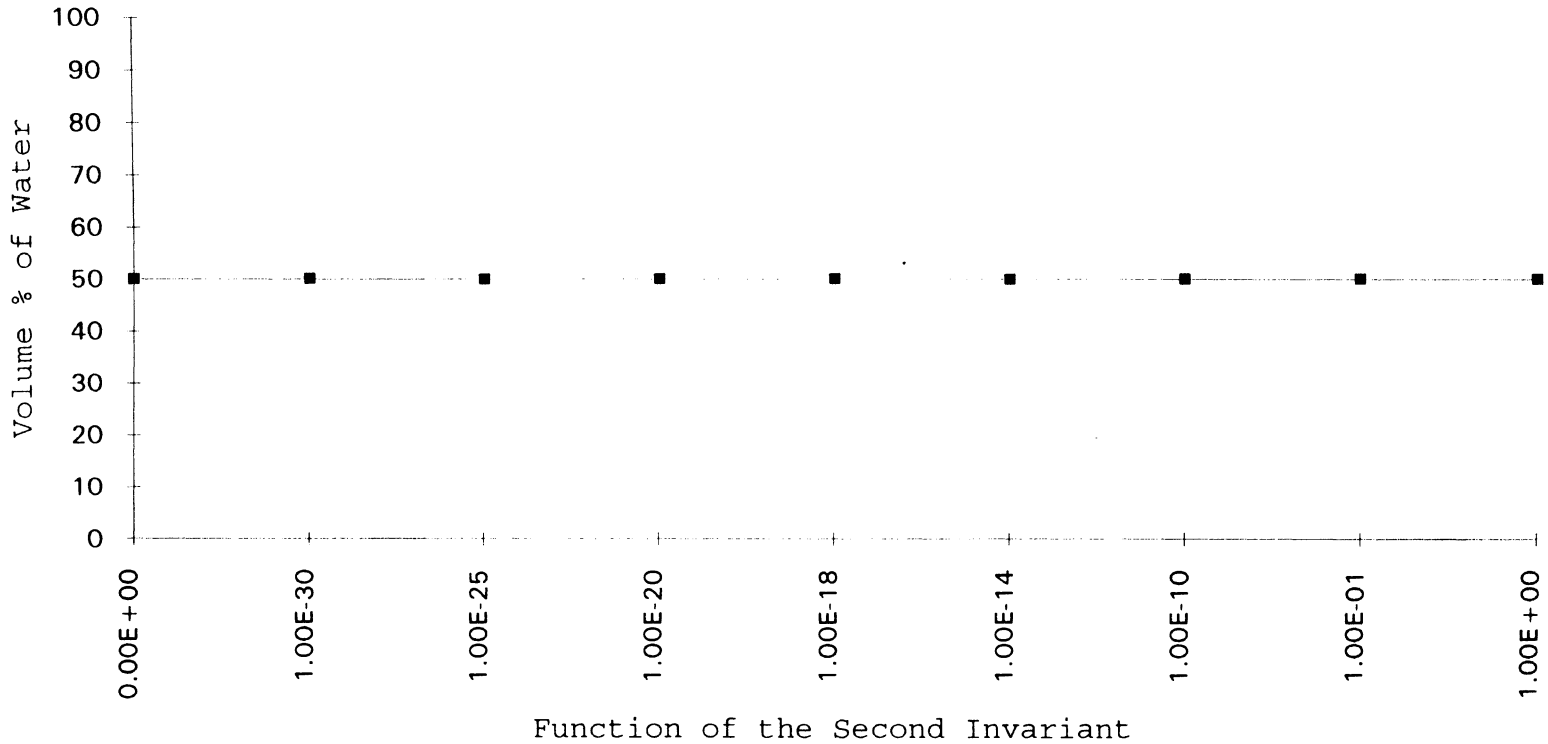

Figure 16. Phase Inversion Map (Equal Second Invariant of Water-in-Oil and Oil-in-Water Emulsion)

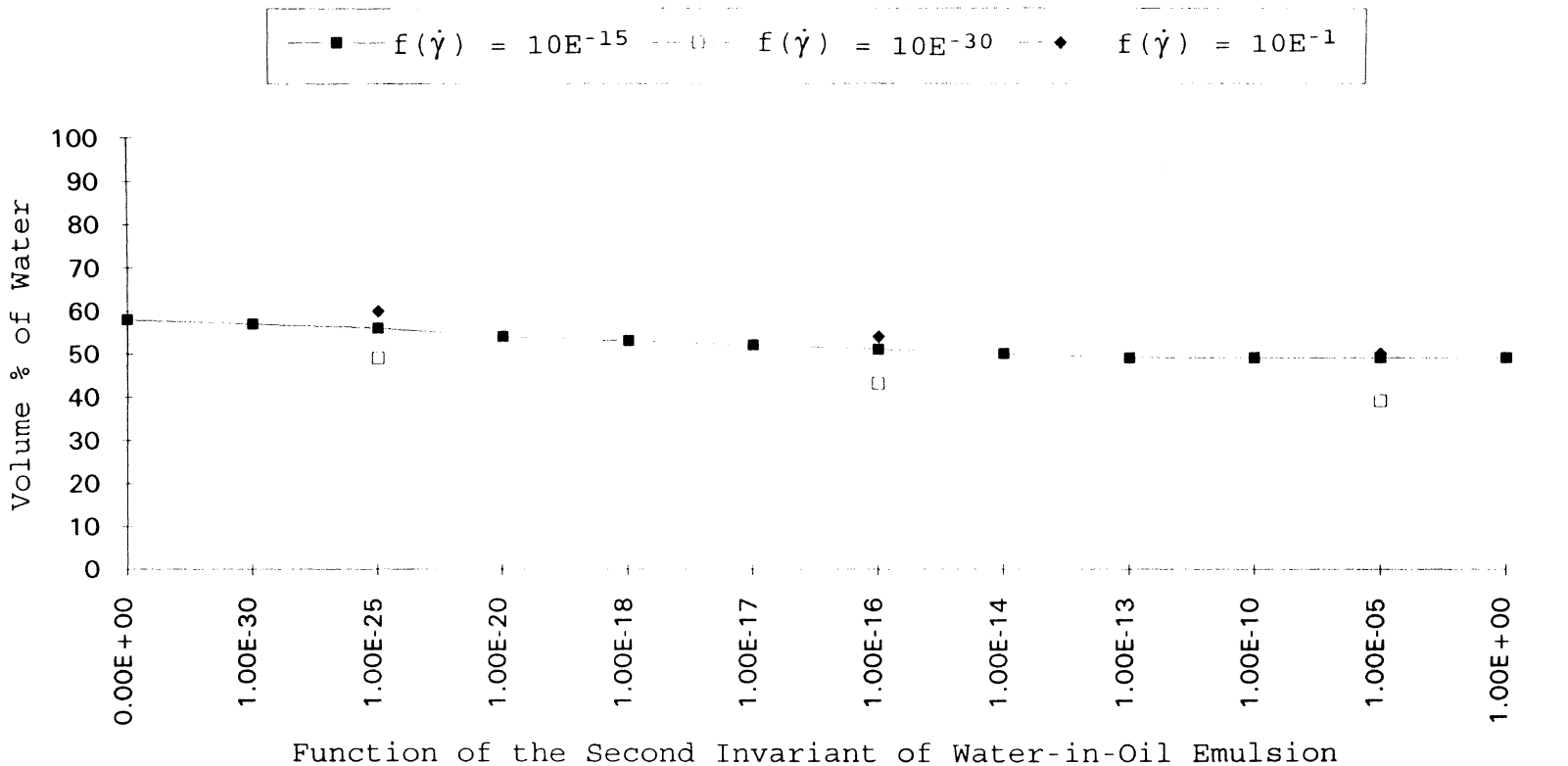

Figure 17. Phase Inversion Map (Different Second Invariant of Water-in-Oil and Oil-in-Water Emulsion)

rate. The second invariant is strongly dependent on the viscosity of the emulsion type. The author can thus conclude that the inversion point of an emulsion system depends on the difference of the viscosities of the water-in-oil and oil-in-water emulsion.

CHAPTER V

CONCLUSIONS AND RECOMMENDATIONS

Conclusions

The main conclusions of the present work can be listed as:

1) A model has been developed to predict the point of phase inversion in an emulsion system as a function of the strength of the flow field and volume of the dispersed phase. This includes the derivations of formulae to calculate the maximum and minimum drop diameters of the emulsion in the annular liquid film and the Monte Carlo numerical technique to determine the distribution of the drop sizes of emulsion in the liquid film.

2) The drop size distribution of the dispersed phase of an emulsion produced by the Monte Carlo method follows a log normal distribution. This result agrees very well with the experimental and empirical work.

3) The strength of the flow field was found to depend on the viscosity of emulsion present in the annular liquid film. The strength of the flow field can be represented as a function of the second invariant of the rate of strain tensor. The second invariant of the emulsion type is a

strong function of the viscosity of the emulsion type. For two emulsion types existing in the liquid film, different values of the strength of the flow field can be calculated.

4) The prediction of the point of emulsion phase inversion was found to depend on the strength of the flow field of both the emulsion types. Inversion occured at 50% for equal value of the strength of the flow field and changed with difference between the strength of the flow fields.

Recommendations

The following suggestions could be recommended for future work in this area:

1) The present work assumes values between 0 and 1 for the strength of the flow field. A relationship needs to be developed for the strength of the flow field. The gas flow rate and fluid properties of the gas and liquid can also be introduced into the equation since they also may have an influence on the drop breakup. Future work could be directed to develop a relationship involving all the above factors to exactly evaluate the strength of the flow field.

2) The fluid properties from the DREAM program could be linked to the present model to calculate the maximum and minimum drop diameters of the dispersed phase.

3) A correlation could be proposed from the Monte Carlo method for the drop size distribution between the

maximum and minimum diameters. The correlation would save much computer time.

REFERENCES

Akashah, S. A, Erbar,J. H & Maddox, R. N. (1982). Two-phase flow calculations incorporating an equation of state. Proceedings of the Sixty-first Annual Convention, Gas Processors Association, Dallas, TX, March 15-17,91.

Batchelor, G. (1959). Theory of Homogeneous Turbulence, Cambridge, 122.

Becher, P. (1966). Emulsions: Theory and practice. 2nd Ed, ACS Monograph series 162, American chemical society, Washington, DC.

Bhatnagar, S. S. (1920). The reversal of phases by electrolytes and the effects of free fatty acids and alkalis on emulsion equilibrium. Journal of Chemical Society, 119, 61.

Bradburn, J. B. (1977). Water production - An Index to corrosion. South Central NACE Meeting, Houston, TX.

Brodnyan, J. G. (1960). Emulsion particle size, II. Journal of Colloid Science, 15, 563-572.

Cayias, J. L., Schechter, R. S., & Wade, W. H. (1975). Adsorption at Interfaces. Mittal, K. L., Ed; ACS Symposium Series 8; American Chemical Society, Washington, DC, 234-247.

Choi, H. J., Cepulis, R. L. & Lee, J. B. (1989). Carbon Dioxide Corrosion of L-80 Grade Tubular in Flowing Oil-Brine Two-Phase Environments. Corrosion, 45, 943-950.

Clay, P. H. (1940). Mechanism of emulsion formation in turbulent flow. Kononklijke Nederlandsche Akademia Van Wetenschappen, 43, 852-865, 979-990.

Crolet, J-L. (1983). Acid Corrosion in Wells: Metallurgical aspects. Journal of Petroleum Technology, 35, 1553-1558.

Crolet, J-L. & Bonis, M. R. (1984). The very nature of the CO_2 Corrosion of Steels om Oil and Gas Wells and

the Corresponding Mechanisms. Oil Gas -European Magazine, 2, 68-76.

Crolet, J-L. & Bonis, M. R. (1989). An Optimized Procedure for Corrosion Testing Under CO_2 and H_2S Gas Pressure. Material Performance, July, 81-86.

De Waard, D. W. & Milliams, D. E. (1975). Carbonic Acid Corrosion of Steel. Corrosion, 31, 177-181.

Epstein, B. (1947). The Mathematical Description of Certain Breakage Mechanisms Leading to the Logarithmico-Normal Distribution. Journal of Franklin Institute, 244, 471-477.

Fang, C. S., Garbar, J. D., Perkins, R. & Reinhardt, J. R. (1989). Computer Model of a Gas Condensate Well containing Carbon Dioxide. Corrosion, Paper No. 465, New Orleans, Louisiana.

Gatze, L. K. & Hausler, R. H. (1984). A Novel Correlation of Tubing Corrosion Rates in Deep, Hot Gas Well with Water and Gas Production Rates. Advances in CO_2 Corrosion, vol 1, National Association of Corrosion Engineers, Houston, TX, 87-102.

Hausler, R. H. (1984). The Mechanism of CO_2 Corrosion in Steel in Hot, Deep Gas Wells. Advances in CO_2 Corrosion, vol 1, National Association of Corrosion Engineers, Houston, TX, 72-86.

Hausler, R. H. & Burke, P. A. (1985). Corrosion Monitoring in Sweet Production: Field Experiences with Iron Counts, Coupons and Calipers. Advances in CO_2 Corrosion, vol 2, National Association of Corrosion Engineers, Houston, TX, 161-192.

Hill, A. D. & Jacks, D. C. (1985). Programs predict pressure for two-phase flow. Oil and Gas Journal, 83(7), 93-96.

Hinze, J. O. (1955). Fundamentals of the hydrodynamic mechanism. Journal of the American Institute of Chemical Engineers, 1, 289.

Ikeda, A., Ueda, M. & Mukai, S. (1984). Advances in CO_2 Corrosion, vol 1, National Association of Corrosion Engineers, Houston, TX, 39-51.

Iyer, R. N., Takenchi, I., & Zamanzadeh, M. & Pichering, H. W. (1991). Hydrogen Sulfide Effect on Hydrogen Entry into Iron -A Mechanistic Study. Corrosion, 46, 460-468.

Johnson, B. V., Choi, H. J. & Green, A. S. (1991). Effects of Liquid Wall Shear Stress on CO2 Corrosion of X-52 C-Steel in Simulated Oilfield Production Environments. Corrosion, Paper No. 573, Cincinnati, Ohio.

Kolmogoroff, A. N. (1949). About Breaking of Drops in Turbulent Flow. Dokl. Akad. Nauk. SSSR, 66, 825.

Kottler, F. (1950). The Distribution of Particle Sizes. Part I & Part II. Journal of Franklin Institute, 250, 339-356, 419-441.

Levich, V. G. (1962). Physicochemical Hydrodynamics, Prentice hall, Eaglewood Cliffs.

Lissant, K. J. (1987). Emulsion & Emulsion Technology, Lissant, K.J., Ed. Marcel Dekker, Newyork.

Liu, Guohai. (1991). A mathematical model for prediction of downhole gas well uniform corrosion in CO_2 and H_2S containing brines. Ph.D Thesis, Chemical Engineering Department, Oklahoma State University.

Liu, Guohai. (1992). Report submitted to the Downhole Consortium Meeting.

Lundberg, Jan. (1987). Rheological model of a dilute emulsion. 42nd Annual Meeting in Anahelm, CA, STLE Transactions, 31(1), 83-90.

Mao, M. L. M. & Marsden, S. S. (1977). Stability of crude oil-in-water emulsion as a function of shear rate, temperature and oil concentration. Journal of Canadian Petroleum Technology, 16, 54-59.

Mahoto, B. K. & Shemilt, L. W. (1968). Effect of Surface Roughness on Mass Transfer. Chemical Engineering Science, 23, 183-185.

Metropolis; N., Rosenbluth; A. W., Rosenbluth; M. N., Teller, A. H. & Teller, E.(1953). Equation of state calculations by fast computing machines. The Journal of Chemical Physics, 21(6), 1087.

Morris, D. R., Sampaleanu, L. P. & Veysey, D. N. (1980). The Corrosion of Steel by Aqueous Solutions of Hydrogen Sulfide. Journal of Electrochemical Society, 127, 1228-1235.

Mugele, R. A. & Evans, H. D. (1951). Droplet Distribution in Sprays. Industrial and Engineering Chemistry, 43(6), 1317-1324.

Pal, Rajinder and Rhodes, Edward. (1989). Viscosity / Concentration Relationships for emulsions. Journal of Rheology, 33(7), 1021-1045.

Pal, Rajinder and Rhodes, Edward. (1985). A novel viscosity correlation for non-newtonian concentrated emulsions. Journal of Colloid and Interface Science, 107(2), 301.

Pal, R., Yan, Y. and Masliyah, J. (1992). Rheology of emulsions. Emulsions: Fundamentals and Applications in the Petroleum Industry, Edited by Schramm, L. L., Advances in Chemistry Series 231, 141.

Payne, J., R and Phillips, C. R. (1985). Laboratory studies of formation and stability of water-in-oil emulsions. Petroleum Spills in the Marine Environment, Lewis Publishers, 4.

Rajagopal, E. S. (1959). Statistical Theory of Particle Size Distributions in Emulsions and Suspensions. Kolloid-Zeitschrift, Band 162, February, 85-92.

Reinhardt, J. R. & Powell, T. S. (1988). Corrosion Reduction in Production Tubing with the Aid of a Phase Equilibrium Model. SPE Production Engineering, 3, 591-596.

Robertson, C. A. (1988). A computer model for predicting the water phase corrosion zone in gas and condensate wells. M.S Thesis, Chemical Engineering Department, Oklahoma State University.

Ross, T. K. & Badhwar, P. K. (1965). The Effect of Surface Roughness upon Electrochemical Process. Corrosion Science, 5, 29-38.

Ross,S. & Kornbrekke, R. E. (1981). Change of morphology of a liquid-liquid dispersion as a stochastic process. Journal of Colloid and Interface Science, 81(1), 58.

Schmitt, G. & Rothmann, B. (1977). Studies on the Corrosion Mechanism of Unalloyed Steel in Oxygen-Free Carbon Dioxide Solutions: Part I. Kinetics of the Liberation of Hydrogen. Werkstoffe and Korrosion, 28, 816-824 in CO_2 Corrosion in Oil and Gas Production, 154-162.

Schramm, L. L. and Smith, R. G. (1985). Colloids Surface , 14, 67-85.

Schramm, L. L. (1992). Petroleum emulsions: Basic principles. Emulsions: Fundamentals and Applications

in the Petroleum Industry, Edited by Schramm, L. L., Advances in Chemistry Series 231, 37.

Schwarz, N. and Bezemer, C. (1956). A new equation for the size distribution of emulsion particles. Kolloid Zeitschrift, 146, 139-151.

Scott, L. S., Hayes, W. B. and Holland, C. D. (1958). The formation of interfacial area in immiscible liquids by orifice mixers. Journal of the American Institute of Chemical Engineers, 4, 346-350.

Sherman, P. (1970). Industrial Rheology, Academic press, London, 138.

Sherman, P. (1968). Emulsion Science; Academic press, Newyork, 316.

Shinoda, K & Kunieda, H. (1983). Phase properties of emulsions: PIT and HLB. Encyclopedia of Emulsion Technology, Becher, P., Ed. Marcel Dekker, Newyork, 337.

Shock, D. A. & Sudbury, J. D. (1951). Prediction of Corrosion in Oil and Gas Wells. World Oil, 133, 180-192.

Smith, F. G. (1982). Controlling Corrosion in Deep South Louisiana Gas Wells. World Oil, 195(6), 77-79.

Smith, D. H. & Lim, Kyung-Hee. (1989). A phase and electrical conductivity study of model oilfield dispersions. Society of Peroleum Engineers 18496, 335.

Smith, D. H & Lim, Kyung-Hee. (1990). Morphology and inversion of dispersions of two fluids in systems of three and four thermodynamic dimensions. Journal of Physical Chemistry, 94, 3746-3752.

Smith, D. H; Covatch, G. C & Lim, Kyung-Hee. (1991). Temperature dependence of emulsion morphologies and the dispersion morphology diagram. Journal of Physical Chemistry, 95(3), 1463-1466.

Takamura, K. (1982). Microscopic structure of athabasca oil sand. Canadian Journal of Chemical Engineering, 60, 538-545.

Takamura, K and Chow, R. S. (1983). Journal of Canadian Petroleum Technology, 22, 22-30.

Taylor, G. I. (1932). The Viscosity of a Fluid Containing Small Drops of Another Fluid. Proceedings of the Royal Society, 201 A, 192-197.

Tuttle, R. N. (1988). Corrosion in Oil and Gas Production. Journal of Petroleum Technology. 39, 756-762.

Tuttle, R. N. (1990). What is Sour Environment?. Journal of Petroleum Technology. 42, 260-362.

Valand, T. & Sjowall, P. A. (1989). Properties and Composition of Surface films Formed on Steel in CO_2-Aqueous Solutions. Electrochimica Acta, 34, 273-279.

Waldrip, H. E and Rowe, J. A. (1958). Variables affecting the corrosivity of oil and gas wells. Corrosion-National Assosiation of Corrosion Engineers, 14, 108.

Wieckowski, A., Ghali, E., Szklarczyk, M., & Sobkowski, J. (1983a). The behavior of Iron Electrode in CO2 Saturated Neutral Electrolyte -I. Electrochemical Study. Electrochimica Acta, 28, 1619-1626.

Wieckowski, A., Ghali, E., Szklarczyk, M., & Sobkowski, J. (1983b). The behavior of Iron Electrode in CO2 Saturated Neutral Electrolyte -II. Radiotracer Study and Corrosion Considerations. Electrochimica Acta, 28, 1627-1633.

Zitter, H. (1973). Corrosion Phenomena in Sour Gas Wells. Erdoel-Erdgas-Zeitschrift, 89(3), 101-106.

APPENDIXES

APPENDIX A

NOMENCLATURE

A	surface area of the deformed drop, cm^2
a	radius of drops, cm
a_{cr}	critical radius of drop, cm
$<D>$	moment of a diameter
D_p	diameter of the pipe, cm
d	diameter of drops, cm
$\bar{d}$	mean drop size in the log-normal function
d_{max}	maximum diameter, cm
d_{min}	minimum diameter, cm
d_s	stable drop size, cm
E_1	energy of initial configuration, dynes.cm
E_2	energy of final configuration, dynes.cm
$\bar{F}$	average of any property of a system
F_j	value of property at j^{th} move
F_σ	surface tension pressure, $dynes/cm^2$
$f(d)$	log-normal function
$g(d)$	function of the drop size
h	height of the deformed drop, cm
$h(\dot{\gamma})$	function of the second invariant
K_f	coefficient in equation (II-19)
l	scale of an eddy, cm

M	number of moves
N	number of drops initially placed in the control volume
NDR	number of drop in one side of the control volume (0.5cm x 0.5cm x 0.5cm) cube
N_{accept}	number of accepted Monte Carlo moves
N_{reject}	number of rejected Monte Carlo moves
P	probability of breakup of drops
Q	dynamic pressure, $g/cm^2.sec^2$
R	universal gas law constant, cm^3 .Pa/mol.K
Re	Reynolds number
R_{crit}	critical distance between drops before coalescence, cm
r_i	radius of the randomly moved drop, i, cm
r_j	radius of the drop nearest to drop i, cm
s	standard deviation of the log-normal function
T	temperature of the emulsion system, K
U	average velocity, cm/sec
$\bar{u}$	mean velocity of drop, cm/sec
u_c	velocity of the continuous phase, cm/sec
u_d	velocity of the dispersed phase, cm/sec
V	volume of the deformed drop, cm^3
V_w	volume of water phase in the control volume, cm^3
v_0	characteristic velocity, cm/sec
v_1, v_2	velocity of the medium at both sides of drop, cm/sec
v_λ	velocity of eddy of scale λ, cm/sec
We	Weber number

We_{crit}	critical Weber number
X_i	x-coordinate of drop index i, cm
X_i^{new}	new x-coordinate of the drop, i after move
X_w	volume fraction of the dispersed water phase
Y_i	y-coordinate of drop index i, cm
Y_i^{new}	new y-coordinate of the drop, i after move
y	distance along x-axis in a vertical flow
Z_i	z-coordinate of drop index i, cm
Z_i^{new}	new z-coordinate of the drop, i after move

Greek symbols

α	constant in equation (III-12)
δ_0	small distance from the wall, cm
ΔE	difference in energy between moves, dynes.cm
Δp	pressure diff across the drop, lb/cm^2
Δq_i	number between 0 and 1
ΔU	change in velocity of scale *l*, cm/sec
ε_0	local energy dissipation per unit mass, dynes.cm/g
ξ	random number between 0 and 1, exclusive
ϕ	dispersed phase volume fraction
$\phi_{\eta_r=100}$	dispersed phase volume fraction at which the relative viscosity is 100
γ	interfacial tension, dynes/cm
$\dot{\gamma}$	second invariant of the rate of strain tensor

$\dot{\gamma}_{liquid}$	second invariant of emulsion type
η_r	relative viscosity of emulsion, dimensionless
λ	scale of small eddy, cm
λ_0	scale of an eddy at which reynolds number of motion is unity, cm
μ_c, μ_d	viscosity of the continuous phase and dispersed phase, g/sec.cm
μ_{liquid}	viscosity of the emulsion type, g/sec.cm
ν	kinematic viscosity, cm^2/sec
ρ	density of eddy, g/cm^3
ρ_c, ρ_d	density of the continuous and dispersed phase, g/cm^3
σ	surface tension, dynes/cm
τ	shear stress, $dynes/cm^2$

APPENDIX B

OPERATING INSTRUCTIONS OF THE CODE

A FORTRAN code was written to predict the point of emulsion phase inversion. The code was used on a rs6000 machine that uses a risc (Reduced Instruction Set Computer) architecture. The machine used was available from the College of Engineering, Architecture and Technology (EN 301, ES Basement).

The instructions for inputting data, compiling and executing the program is given below. The input data should be entered to the program such as, Minimum diameter, Maximum diameter, Second invariant of the water-in-oil & oil-in-water emulsion, Number of moves and the volume fraction of water. The output is written in the files that are created during execution of the program. The program should be compiled after making the input data changes using

xlf -o *executable filename* source filename

The above command creates an executable file which could be typed to execute the program. The running time of the code is lengthy and hence the program could be run in the background using the following command,

nice nohup *executable filename* &

The program runs roughly for 6-7 hours for 100,000 moves. The commented computer program is listed in the next few pages.

APPENDIX C

COMPUTER CODE LISTING TO PREDICT THE POINT OF EMULSION PHASE INVERSION

```
C     THIS PROGRAM IS THE APPROACH WHICH USES THE ENERGY LEVELS
C     FROM DROP SIZE DISTRIBUTION AS AN INDEX TO PREDICT THE EMULSION
C     PHASE INVERSION.  THE MONTE CARLO METHOD IS USED TO DETERMINE
C     THE DROP SIZE DISTRIBUTION OF THE EMULSIONS.

C     NOMENCLATURE

C     X,Y,Z =  THE THREE AXES TO REPRESENT THE DROP
C     DIA   =  DIAMETER OF THE DROP (CM)
C     NACC  =  NUMBER OF ACCEPTED MOVES
C     NREJ  =  NUMBER OF REJECTED MOVES
C     NTOT  =  TOTAL NUMBER OF MOVES
C     G     =  GRAVITATIONAL CONSTANT
C     ENGY1 =  ENERGY BEFORE THE MONTE CARLO MOVE
C     ENGY2 =  ENERGY AFTER THE MONTE CARLO MOVE
C     GAMWA =  SURFACE TENSION OF WATER
C     XNEW  =  NEW POSITION OF DROP IN THE X-DIRECTION
C     YNEW  =  NEW POSITION OF DROP IN THE Y-DIRECTION
C     ZNEW  =  NEW POSITION OF DROP IN THE Z-DIRECTION
C     RCRIT =  CRITICAL DISTANCE BETWEEN DROPS BEFORE THEY COMBINE
C     NEAR  =  NEAREST DROP TO THE SELECTED DROP WITH WHICH IT COMBINES
C     TOVOL =  TOTAL VOLUME OF THE COMBINED DROPS
C     BREAK =  DIAMETER OF DROP AFTER BREAKAGE OCCURS
C     DELEN =  DIFFERENCE IN THE ENERGY BEFORE AND AFTER MOVES
C     RATIO =  RATIO OF THE ACCEPTANCE TO REJECTION
C     D1,D2 =  FIRST AND SECOND MOMENTS OF THE DIAMETER
C     D3,D4 =  THIRD AND FOURTH MOMENTS OF THE DIAMETER

C     THIS IS THE MAIN PROGRAM WHICH SCANS FOR THE VOLUME FRACTION OF
C     WATER AND ASSIGNS VALUES FOR MAXIMUM AND MINIMUM DIAMETERS.

      COMMON /ALI/  PIPE_LGTH, CON_ZONE, PDIA, DELTA
      COMMON /A2/ VWATER, VOIL
      COMMON /AM0C/ ENGY_WATDIS, ENGY_OILDIS

      OPEN(UNIT=1,FILE='CASESUM.OUT')
      CON_ZONE = 1000.
      PDIA =       5.
      PIPE_LGTH = 10000.
      DELTA = 0.08
      VTOTAL = 3830.22
      PER_WAT = 50.
      ALOC = CON_ZONE

  800 ALOC = ALOC + 100
      IF(ALOC.GT.PIPE_LGTH) WRITE(*,*) 'NO CORROSION IN THIS WELL'
      VWATER = 3830.22*PER_WAT/100.
```

```
      VOIL = VTOTAL - VWATER
      WRITE(1,*) 'THE VOLUMES OF WATER AND OIL ARE',VWATER,'&',VOIL
      VOL_FRC = VWATER/VTOTAL
      DMIN = 0.04
      DMAX = 0.08

      CALL AMC (DMIN, DMAX)

      A = 0
         IF(ENGY_WATDIS.LE.ENGY_OILDIS) THEN
         WRITE(1,*) 'W/0 IS THE STABLE EMULSION'
         WRITE(1,*) 'PER_WAT=',PER_WAT
         WRITE(1,*) 'ENERGY WAT DISP=',ENGY_WATDIS
         WRITE(1,*) 'ENERGY OIL DISP=',ENGY_OILDIS
         STOP
      ELSE
         WRITE(1,*) 'O/W IS THE STABLE EMULSION'
         WRITE(1,*) 'EMULSION INVERSION = ',PER_WAT
         WRITE(1,*) 'ENERGY WAT DISP=',ENGY_WATDIS
         WRITE(1,*) 'ENERGY OIL DISP=',ENGY_OILDIS
      ENDIF
      STOP
      END


      SUBROUTINE AMC (DMIN, DMAX)

C     THE MONTE CARLO APPROACH TO DETERMINE THE DROP SIZE DISTRIBUTION
C     USING RANDOM NUMBERS.  THE DIMENSION OF THE CONTROL VOLUME OF THE
C     CUBE IS 0.5CM X 0.5CM X 0.5CM.  ALL DROPS ARE OF THE SAME
C     DIAMETER, THE MINIMUM DIAMETER.  THE WATER IS INITIALLY CONSIDERED
C     AS THE DISPERSED DROPLETS.

      REAL INVOL
      COMMON /C/ N
      COMMON /ALI/  PIPE_LGTH, CON_ZONE, PDIA, DELTA
      COMMON /A2/ VWATER, VOIL
      COMMON /AM0C/ ENGY_WATDIS, ENGY_OILDIS

      DOUBLE PRECISION BREAK, CHECK(10), N_CORNER(10), DBAR(10)
      DOUBLEPRECISION DIA(50000),X(50000),Y(50000),Z(50000)
      DOUBLEPRECISION SINV_CON
      DOUBLEPRECISION DEL(50000)

      OPEN(UNIT=2,FILE='CASEA.OUT')
      OPEN(UNIT=4,FILE='CASEA.ENG')
      OPEN(UNIT=7,FILE='CASEA.HIS')

      A     = 0
      GAMWA = 30.
      SINV_CON= 1.E-30
 1001 R     = 8.314E+07
      DELTD = 0.5
      DSTAB = .04
      T     = 100.
      KOUNT = 0
      M     = 1
      MOVES = 1
      L     = 0
      PD1   = 0
      PD2   = 0
      PD3   = 0
      PD4   = 0
      CON   = 11./21.
```

```
      LDR_REM = 0
      DUMMY = 0
      KS    = 0
      NACC  = 0
      NREJ  = 0
      NTOT  = 0
      SUM   = 0
      IF(A.EQ.1) GOTO 1000

C     THIS PART CALCULATES THE SIMULATED NUMBER OF DROPS FOR THE
C     CONTROL VOLUME OF (0.5)**3

      AMOL_FRC = VWATER/(100.*12.*2.54*DELTA*(22./7.)*PDIA)
      SIM_VWATER = 0.5**3*AMOL_FRC
      WRITE(1,*) 'AMOL_FRC(WATER) ', AMOL_FRC
      N = SIM_VWATER/(CON*DSTAB**3)
      WRITE(1,*) 'NTRUE',N
      NTRUE = N
      GOTO 1010

 1000 AMOL_FRC = VOIL/(100.*12.*2.54*DELTA*(22./7.)*PDIA)
      SIM_VOIL = 0.5**3*AMOL_FRC
      WRITE(1,*) 'AMOL_FRC(OIL) ', AMOL_FRC
      N = SIM_VOIL/(CON*DSTAB**3)
      WRITE(1,*) 'NTRUE',N
      NTRUE = N

 1010 CALL SIDEN (DR,N)
      WRITE (1,*) 'THE VALUE OF DR IS ',DR
      NDR = INT(DR)+1
      N = 1

C     INITIAL POSITIONS OF THE DROPS IN THE CUBE

      DO 10 I = 1,NDR
      DO 11 J = 1,NDR
      DO 12 K = 1,NDR
      X(N) = (REAL(I)-1.)*0.5/(NDR-1)
      Y(N) = (REAL(J)-1.)*0.5/(NDR-1)
      Z(N) = (REAL(K)-1.)*0.5/(NDR-1)
      DIA(N) = .04
      N = N+1
 12   CONTINUE
 11   CONTINUE
 10   CONTINUE

      CONST = 0.5/(2.*(NDR-1))

      DO 13 I = 1,NDR-1
      DO 14 J = 1,NDR-1
      DO 15 K = 1,NDR
      X(N) = REAL(I)*0.5/(NDR-1)-CONST
      Y(N) = REAL(J)*0.5/(NDR-1)-CONST
      Z(N) = (REAL(K)-1.)*0.5/(NDR-1)
      DIA(N) = .04
      N = N+1
 15   CONTINUE
 14   CONTINUE
 13   CONTINUE

      DO 113 I = 1,NDR-1
      DO 114 J = 1,NDR
      DO 115 K = 1,NDR-1
      X(N) = REAL(I)*0.5/(NDR-1)-CONST
```

```
      Y(N) = (REAL(J)-1.)*0.5/(NDR-1)
      Z(N) = REAL(K)*0.5/(NDR-1)-CONST
      DIA(N) = .04
      N = N+1
 115  CONTINUE
 114  CONTINUE
 113  CONTINUE

      DO 213 I = 1,NDR
      DO 214 J = 1,NDR-1
      DO 215 K = 1,NDR-1
      X(N) = (REAL(I)-1.)*0.5/(NDR-1)
      Y(N) = REAL(J)*0.5/(NDR-1)-CONST
      Z(N) = REAL(K)*0.5/(NDR-1)-CONST DIA(N) = .04
      N = N+1
 215  CONTINUE
 214  CONTINUE
 213  CONTINUE

      N = N-1
      DO I = NTRUE+1, N
      X(I) = 0
      Y(I) = 0
      Z(I) = 0
      DIA(I) = 0
      ENDDO
      N = NTRUE

C     ENERGY IN THE INITIAL CONFIGURATION

      SUM1 = 0
      INVOL = 0
      DO 20 K = 1,N
      INVOL = INVOL + CON*DIA(K)**3
      SUM1 = SUM1 + DIA(K)**2
 20   CONTINUE
      ENGY1 = SUM1*(22./7.)*GAMWA
      WRITE(4,*) DUMMY, ENGY1

C     RANDOM WALK IN ALL DIRECTIONS

      I = N-100
 90   AX = X(I)
      AY = Y(I)
      AZ = Z(I)
      DI = DIA(I)
      XNEW = X(I)+(.25-RAND()/2.)*DELTD
      YNEW = Y(I)+(.25-RAND()/2.)*DELTD
      ZNEW = Z(I)+(.25-RAND()/2.)*DELTD
      IF(XNEW.LT. 0) XNEW = -XNEW
      IF(XNEW.GT..5) XNEW = 1.0-XNEW
      IF(YNEW.LT. 0) YNEW = -YNEW
      IF(YNEW.GT..5) YNEW = 1.0-YNEW
      IF(ZNEW.LT. 0) ZNEW = -ZNEW
      IF(ZNEW.GT..5) ZNEW = 1.0-ZNEW

C     DISTANCE BETWEEN THE DROP AND ITS NEAREST NEIGHBOUR

      RCRIT = 0.01
      DO 30 J = 1,N
      IF((I.EQ.DEL(J)).or.(I.EQ.J)) GOTO 30
      IF(ABS(XNEW-X(J)).GT.RCRIT) GOTO 30
      IF(ABS(YNEW-Y(J)).GT.RCRIT) GOTO 30
      IF(ABS(ZNEW-Z(J)).GT.RCRIT) GOTO 30
```

```
      IF (RAND().LT.TEST) GOTO 70
      X(I)    =  AX
      Y(I)    =  AY
      Z(I)    =  AZ
      DIA(I)  =  DI
      X(J)    =  BX
      Y(J)    =  BY
      Z(J)    =  BZ
      DIA(J)  =  DJ
      MOVES   =  MOVES - 1
      DEL(M-1) = 0
      NREJ    =  NREJ+1
      GOTO 80

 70   NACC   = NACC+1
      WRITE(4,*) MOVES, ENGY2
 80   ENGY1 = ENGY2
      NTOT   = NTOT+1

C     TESTING FOR THE CONVERGENCE CRITERION BASED ON THE MOMENTS OF
C     THE DIAMETERS AT THE END OF EVERY 1000 MOVES.  THE CONVERGENCE
C     IS CODED BUT NOT USED.  100,000 MOVES WERE MADE FOR CONVERGENCE
C     TO OCCUR.

      GO TO 105
      KOUNT = KOUNT+1
      IF((KOUNT/ICOUNT-REAL(KOUNT)/REAL(ICOUNT)).NE.0) THEN
          I = J
          MOVES = MOVES + 1
          GOTO 90
      ELSE
      ENDIF

      D1 = 0
      D2 = 0
      D3 = 0
      D4 = 0
      DO 100 K = 1,N
      D1 = D1+DIA(K)
      D2 = D2+DIA(K)**2
      D3 = D3+DIA(K)**3
      D4 = D4+DIA(K)**4
 100  CONTINUE

      IF (ABS((D1 - PD1)/D1)*100 .GT. 10) GOTO 105
      IF (ABS((D2 - PD2)/D2)*100 .GT. 10) GOTO 105
      IF (ABS((D3 - PD3)/D3)*100 .GT. 10) GOTO 105
      IF (ABS((D4 - PD4)/D4)*100 .GT. 10) GOTO 105

C     ELIMINATING ALL THE DROP INDEXES OF DIAMETER ZERO

 999  WRITE(*,*) 'N =',N
      DO 167 K = 1,N
      IF (DIA(K).EQ.0) GOTO 167
      LDR_REM = LDR_REM + 1
      DIA(LDR_REM) = DIA(K)
 167  CONTINUE
      WRITE(*,*) 'LDR_REM=',LDR_REM

C     SORTING THE FINAL DROPS ACCORDING TO THE INCREASE IN DIAMETERS

      DO 510 I = 1,LDR_REM
      DO 520 J =1,I
      IF(DIA(I).GT.DIA(J))GOTO 520
```

```
      TEMP = DIA(I)
      DIA(I) = DIA(J)
      DIA(J) = TEMP
  520 CONTINUE
  510 CONTINUE
      WRITE(2,330) (DIA(I),I=1,LDR_REM)

C     CALCULATING THE FINAL VOLUME AND THE NUMBER OF DROPS PRESENT
C     IN EACH SECTION OF VOLUME PERCENTAGE 12.5%.

      VOL3 = 0
      DO K = 1, LDR_REM
      VOL3 = VOL3 + CON*DIA(K)**3
      ENDDO
      DO II = 1,8
      CHECK(II) = REAL(II)/8.*VOL3
      ENDDO
      VOL3 = 0
      II = 1
      KPREV = 0
      SUMP = 0

      DO 1167 K = 1, LDR_REM
      VOL3 = VOL3 + CON*DIA(K)**3
      SUM = SUM + DIA(K)
      IF(VOL3.GE.CHECK(II)) THEN
           N_CORNER(II) = K-KPREV
           DBAR(II) = (SUM - SUMP)/N_CORNER(II) KPREV = K
           SUMP = SUM
           II = II + 1
      ELSE
      ENDIF
 1167 CONTINUE

      DO II = 1,8
      WRITE (1,*)  II, N_CORNER(II), DBAR(II)
      ENDDO

C     WRITING THE DROP FREQUENCY ACCORDING TO THEIR DIAMETERS IN
C     ORDER TO CONSTRUCT A HISTOGRAM OF THE DROP SIZE DISTRIBUTION

  639 DO I = 1, LDR_REM
      IF ((DIA(I).GT.0.020).AND.(DIA(I).LT.0.025))  KA = KA+1
      IF (DIA(I).LT.0.030)  KB = KB+1
      IF (DIA(I).LT.0.035)  KC = KC+1
      IF (DIA(I).LT.0.040)  KD = KD+1
      IF (DIA(I).LT.0.045)  KE = KE+1
      IF (DIA(I).LT.0.050)  KF = KF+1
      IF (DIA(I).LT.0.055)  KG = KG+1
      IF (DIA(I).LT.0.060)  KH = KH+1
      IF (DIA(I).LT.0.065)  KO = KO+1
      IF (DIA(I).LT.0.070)  KP = KP+1
      IF (DIA(I).LT.0.075)  KQ = KQ+1
      IF (DIA(I).LT.0.080)  KR = KR+1
      ENDDO

      WRITE(7,*)  KS,    '  ', '0.020'
      WRITE(7,*)  KA,    '  ', '0.020'
      WRITE(7,*)  KA,    '  ', '0.025'
      WRITE(7,*)  KB-KA,'  ', '0.025'
      WRITE(7,*)  KB-KA,'  ', '0.030'
      WRITE(7,*)  KC-KB,'  ', '0.030'
      WRITE(7,*)  KC-KB,'  ', '0.035'
      WRITE(7,*)  KD-KC,'  ', '0.035'
```

```
      WRITE(7,*)  KD-KC,'   ', '0.040'
      WRITE(7,*)  KE-KD,'   ', '0.040'
      WRITE(7,*)  KE-KD,'   ', '0.045'
      WRITE(7,*)  KF-KE,'   ', '0.045'
      WRITE(7,*)  KF-KE,'   ', '0.050'
      WRITE(7,*)  KG-KF,'   ', '0.050'
      WRITE(7,*)  KG-KF,'   ', '0.055'
      WRITE(7,*)  KH-KG,'   ', '0.055'
      WRITE(7,*)  KH-KG,'   ', '0.060'
      WRITE(7,*)  KO-KH,'   ', '0.060'
      WRITE(7,*)  KO-KH,'   ', '0.065'
      WRITE(7,*)  KP-KO,'   ', '0.065'
      WRITE(7,*)  KP-KO,'   ', '0.070'
      WRITE(7,*)  KQ-KP,'   ', '0.070'
      WRITE(7,*)  KQ-KP,'   ', '0.075'
      WRITE(7,*)  KR-KQ,'   ', '0.075'
      WRITE(7,*)  KR-KQ,'   ', '0.080'
      WRITE(7,*)  KS,    '   ', '0.080'

      WRITE(2,*) 'N REJECT', NREJ, 'N ACCEPT', NACC, 'N TOTAL', NTOT
      WRITE(2,*) 'THE INITIAL VOLUME IS =', INVOL
      WRITE(2,*) 'THE TOTAL VOLUME =', VOL3
      WRITE(2,*) 'VOLUME FRACTION =', INVOL/(.5**3)
      WRITE(2,*) 'PROGRAM TERMINATED BY MOMENTS CONDITION'

      ENGY_OILDIS = ENGY2
      IF(A.EQ.1) RETURN
      A=1.
      ENGY_WATDIS = ENGY2
      SINV_CON = 1.E-30

      DO I = 1,N
      X(I) = 0
      Y(I) = 0
      Z(I) = 0
      DIA(I)= 0
      DEL(I) = 0
      ENDDO

      CLOSE(UNIT=2)
      CLOSE(UNIT=3)
      CLOSE(UNIT=4)
      CLOSE(UNIT=7)

      OPEN(UNIT=2,FILE='CASEB.OUT')
      OPEN(UNIT=4,FILE='CASEB.ENG')
      OPEN(UNIT=7,FILE='CASEB.HIS')
      GOTO 1001

105   I = J
      MOVES = MOVES + 1
      IF(MOVES.GT.50000) GOTO 999
      GOTO 90
      END


      SUBROUTINE RANBRK (DMAX,DMIN,I,J,DIA,X,Y,Z,SINV_CON)

      COMMON /C/ N
      DOUBLEPRECISION DIA(50000),X(50000),Y(50000),Z(50000)
      DOUBLEPRECISION BRDIA

      DSTAB = .04
      CON = 11./21.
```

```
      TMP = 0
      KK = 1
      DO 125 K = 1, N
      IF (DIA(K).LE.(0.05040)) GOTO 125
      L = TMP
      PROB = SINV_CON * EXP(-(4.6*(DMAX-DIA(K)))/(DMAX - DMIN))
      IF(RAND().LT.PROB) GOTO 130
      TMP = K
      GOTO 125
  130 BRDIA = (0.5*DIA(K)**3)**(1./3.)
      DIA(K) = BRDIA
      DIA(KK+N) = BRDIA
      X(KK+N) = (X(K)+X(L))/2.
      Y(KK+N) = (Y(K)+Y(L))/2.
      Z(KK+N) = (Z(K)+Z(L))/2.
      KK = KK+1
      TMP = K
      NN = KK+N
  125 CONTINUE
      IF (NN.EQ.0) GOTO 126
      N = NN
  126 NN = 0
      L = 0
      RETURN
      END

      SUBROUTINE SIDEN (DR,N)

C     BISECTION METHOD TO FIND THE ROOT OF AN EQUATION

      EXTERNAL F
      COMMON /Z1/ Z

      Z          = N
      XL       = 1.
      XR       = 25.
      ERLIM    = .1
      I = 0
  705 IF(F(XL)*F(XR).LE.0) GOTO 710
      XR = XL
      XL = TEMP
      GOTO 720
  710 IF(ABS(XL-XR).LE.(2*ERLIM)) GOTO 730
      TEMP = XL
  720 I = I+1
      XL = (XL+XR)/2.
      GOTO 705
  730 ROOT = (XL+XR)/2.
      DR =  ROOT
  740 FORMAT (4X,F8.4,4X,F8.4,4X,F8.4,4X,F8.4)
      RETURN
      END

      REAL FUNCTION F(X)
      COMMON /Z1/ Z
      F = 4.*X**3-6.*X*X+3.*X-Z
      RETURN
      END
```

VITA

Sivakumar Sambasivam

Candidate for the Degree of

Master of Science

Thesis: A MODEL TO PREDICT OIL/WATER EMULSION PHASE INVERSION IN THE DOWNHOLE ENVIRONMENT

Major Field: Chemical Engineering

Biographical:

Personal Data: Born in Madras, India, July 29,1969, the son of Sambasivam V. and Jayalakshmi S.

Education: Graduated from St. Anthony's Higher Secondary School, Coonoor, India, in May 1986; received Bachelor of Technology Degree in Chemical Engineering from Bharathiar University at Coimbatore in May, 1990; completed requirements for the Master of Science degree at Oklahoma State University in May, 1994.

Professional Experience: Research Assistant, Department of Chemical Engineering, Oklahoma State University, August, 1991, to December, 1993; Project Engineer, South India Viscose, Coimbatore, India, June 1990 to July 1991.